SYNTHESIS AND SINTERING 6 (2026) 172–202

Available online at www.synsint.com

Synthesis and Sintering

ISSN 2564-0186 (Print), **ISSN** 2564-0194 (Online)

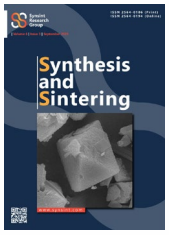

Review article

Engineering birefringence in polymers and polymer-based nanocomposites: Mechanisms, characterization, control, and applications

Ali Borchloo *

Center for Nanoscience and Nanotechnology, Institute for Convergence Science & Technology, Sharif University of Technology, Tehran 14588-89694, Iran

ABSTRACT

Birefringence is a key optical property of polymers and polymer nanocomposites, influencing the performance of optical, photonic, and electro-optical devices. Precise control of birefringence is essential for polarization optics, optical communication, flexible electronics, smart materials, and stress analysis. Although previous reviews have addressed specific aspects of polymer birefringence, a framework linking molecular and structural origins to processing, nanofiller engineering, characterization, and material design remains limited. This review addresses this gap by providing an integrated and critical analysis of the mechanisms, theoretical models, processing-structure relationships, nanofiller effects, characterization approaches, and emerging applications of birefringence in polymeric systems. Attention is given to polymer chain orientation, crystallinity, molecular anisotropy, residual stress, phase morphology, and the effects of nanofiller dispersion, orientation, concentration, and surface functionalization on refractive-index modulation and optical anisotropy. Theoretical approaches, including the Lorentz-Lorenz equation, stress-optical relationship, and Abbe number, are examined to clarify the relationships among material structure, processing, refractive index, and birefringence. Advanced characterization techniques, including polarized optical microscopy, interferometry, ellipsometry, polarimetry, conoscopic analysis, and electro-optic and magneto-optic methods, are compared in terms of their principles, capabilities, and limitations. Recent advances in optical sensors, waveguides, optical films, liquid crystal displays, biomedical devices, and multifunctional smart materials are highlighted. Unlike earlier reviews that primarily emphasize individual mechanisms, materials, or applications, this review establishes an integrated structure-processing-property perspective. It further provides practical guidance on polymer architectures, processing conditions, nanofiller characteristics, surface-engineering strategies, and characterization methods to achieve targeted birefringence. Finally, current challenges, knowledge gaps, and future research directions are identified to support the rational design of next-generation high-performance optical and photonic polymer nanocomposites for emerging applications in high-performance optical and photonic devices.

KEYWORDS

Birefringence
Polymer-based nanocomposites
Optical anisotropy
Refractive index
Nanofillers

OPEN ACCESS

* Corresponding author. *E-mail address:* ali.borchloo77@sharif.edu (A. Borchloo)
Received 27 July 2026; Received in revised form 23 August 2026; Accepted 28 August 2026.

https://doi.org/10.53063/synsint.2026.63364

1. Introduction

Polymers have become a major type of modern engineering material over the past few decades, playing an important role in many manufacturing settings. Their inherent advantages, including reduced mass, robust chemical resistance, straightforward processing, architectural versatility, and economical production, have positioned them as viable substitutes for legacy materials such as metals and ceramics [1]. Moreover, the tunable nature of their molecular and chemical architecture allows for targeted refinement to meet the rigorous demands of specialized domains, including optoelectronic devices, energy systems, biomedical platforms, and sensor technologies. As a result, a substantial body of ongoing research is dedicated to advancing polymer capabilities and functional outcomes, with a pronounced emphasis on polymer-based composite systems [2].

Polymer composites are hybrid systems composed of a polymeric matrix integrated with inorganic or organic reinforcements at either nanometer or micrometer dimensions. Such fillers encompass metallic-semiconducting nanostructures, ceramic particulates, carbonaceous fibers, and discrete organic or inorganic nanoparticles, whose dispersion within the polymer matrix can range from relatively uniform distributions to aggregated or agglomerated states depending on filler characteristics, surface interactions, concentration, and processing conditions [3]. The spatial distribution, orientation, and degree of aggregation of these fillers can substantially influence the optical anisotropy and birefringence of the resulting composite. The concurrent exploitation of the intrinsic optical merits of inorganic constituents and the facile processing and mechanical compliance of polymers permits the engineering of materials exhibiting tailored optical and electronic responses. Consequently, critical parameters, namely the refractive index, light transmittance, absorptivity, and optical bandgap, can be adjusted through appropriate control of the composite composition and microstructure. Owing to this versatility, polymer composites have garnered intense research interest within the materials science and nanotechnology communities recently [2, 4].

A particularly strategic and rapidly evolving domain for the deployment of polymer composites lies in the advancement of green energy platforms and optoelectronic devices. In response to the pressing global issues associated with fossil fuel depletion and the critical need for renewable energy infrastructure, extensive research has focused on incorporating polymeric materials into organic photovoltaics, light-emitting diodes (LEDs), optical waveguide sensors, and supercapacitors [5]. The intrinsic attributes of polymers, specifically their low mass, economic viability, and the tailorability of their electronic band structure, render them highly promising media for photon harvesting and energy transduction. Polymer composites embedded with metallic or semiconductor dopants have demonstrated marked improvements in photovoltaic and optoelectronic performance, attributable to enhanced optical absorption cross-sections and a narrowed optical bandgap [2, 4, 6].

Polymers consist of extended macromolecular chains comprising repeating monomeric subunits, an architecture that confers a distinctive amalgamation of physical and chemical characteristics. Their inherently low specific gravity provides a mass advantage over conventional metals and ceramics, making them particularly well-suited for weight-sensitive engineering applications [7]. The chemical resistance of polymers varies significantly depending on their molecular structure and the specific environmental conditions. While certain polymers such as PTFE and PEEK exhibit excellent stability against corrosive, acidic, or alkaline media, others may undergo degradation under such conditions [2]. A further salient feature is their facile processability, enabling fabrication into intricate geometries through techniques such as injection molding, extrusion, or solution-based deposition [8]. Polymers are a very cost-effective material class for modern industry because there are so many precursor feedstocks available, and the manufacturing processes are so cheap. Consequently, polymers have attained a critical role not only in conventional sectors like packaging and automotive manufacturing but also within cutting-edge fields including optoelectronic devices, photovoltaic energy conversion, and nanotechnology [6].

A highly efficacious approach for broadening the functional utility of polymers involves tailoring their intrinsic characteristics via the integration of fillers or nanoscale additives. In this methodology, discrete entities spanning metallic, semiconducting, ceramic, or organic classifications are homogeneously embedded within the host polymer network to augment the material's physical, mechanical, or optical response [9]. Illustratively, noble metal nanoparticles (e.g., Ag, Au, Cu) serve to amplify both electrical conduction pathways and photon absorption cross-sections; semiconductor nanocrystals (e.g., TiO_2, ZnO, CdS) afford precise control over the optical bandgap and refractive index modulation, whereas inorganic or organic particulates (e.g., SiO_2, Al_2O_3) bolster optical clarity and structural rigidity. Concurrently, carbonaceous reinforcements, including carbon fibers and nanotubes, impart enhanced electro-thermal transport characteristics, while ceramic constituents (e.g., $BaTiO_3$, AlN) elevate the dielectric permittivity and thermal endurance of the system [10–12]. This heterogeneous, multi-phase architecture, which capitalizes on the complementary attributes of the polymeric medium and the embedded phase, defines the foundational principle of polymer composites, a class of materials now central to cutting-edge investigations in photonic and electronic materials science [9, 13].

A primary route toward augmenting the performance envelope of polymers lies in the integration of particulate matter at nanometer or micrometer dimensions into the host polymeric matrix, a procedure commonly designated as doping or filling. This strategy yields substantial modifications in the electrical, photonic, mechanical, and thermal signatures of the base polymer [14, 15]. Illustrative examples include noble metal nanoparticles (Ag, Au), which amplify both charge transport and optical absorbance, and semiconductor species (TiO_2, ZnO), which enable precise manipulation of the bandgap energy and refractive index. Incorporation of SiO_2 or Al_2O_3 reinforcements serves to elevate mechanical robustness, whereas carbonaceous additives, namely fibers or nanotubes, enhance both electrical and thermal conduction pathways. Additionally, ceramic inclusions such as $BaTiO_3$ augment the dielectric permittivity, thereby refining the electro-optical response of the composite system. The resultant multi-component architectures, which collectively harness a diverse array of physical and optical functionalities, are formally classified as polymer composites [2, 4, 9].

1.1. Defining birefringence (Δn): The index ellipsoid

When light enters an optically anisotropic material, rather than following a single refracted path, it splits into two refracted rays [16]. In optically anisotropic materials, an incident light beam splits into two refracted rays: the ordinary ray, which obeys Snell's law with a

constant refractive index independent of propagation direction, and the extraordinary ray, whose refractive index varies with direction relative to the optical axis and thus follows a modified form of Snell's law that accounts for this angular dependence [17].

The first ray, termed the ordinary ray, possesses a refractive index that is invariant with direction and fully complies with Snell's Law. The velocity and propagation path of this ray are independent of its polarization state; consequently, its behavior within the anisotropic medium mirrors that of light in an isotropic environment [17].

In contrast, the second ray, designated the extraordinary ray, exhibits a refractive index that depends upon both the direction of propagation and the polarization of the light. Unlike the ordinary ray, the extraordinary ray does not adhere to Snell's Law, and its propagation trajectory within the material varies according to the crystallographic orientation or the alignment of molecular chains [18]. As these two rays possess orthogonal polarizations, their respective electric field vectors oscillate in mutually perpendicular planes. This characteristic constitutes the fundamental basis for numerous optical applications, including polarizing filters, wave plates, and light-modulation systems employing birefringent materials. A schematic representation of this phenomenon, depicting incident light and its division into two rays with orthogonal polarizations, is presented in Fig. 1 [17].

For uniaxially oriented polymeric materials, birefringence is defined as $\Delta n = n_e - n_o$, where n_e is the refractive index along the extraordinary axis (parallel to the polymer chain orientation or optical axis) and n_o is the refractive index along the ordinary axis (perpendicular to it) [19]. This differential magnitude is fundamentally a manifestation of the optical anisotropy inherent within the polymer structure and is directly correlated with the degree of order or the orientation of molecular chains. Any alteration in this structural order, whether induced by mechanical processing such as drawing or molding or by thermal factors, can significantly modify the magnitude of birefringence. Precise control of birefringence plays a critical role in the design and performance of numerous photonic devices [20]. In systems such as optical waveguides, polarization filters, liquid crystal displays (LCDs), and optical sensors, excessive or undesirable birefringence can induce phase shifts, beam distortion, and disruption of optical transmission or interference. Therefore, meticulous engineering of the polymer structure and management of internal stresses are essential to achieving optimal performance [17].

1.2. Origins of anisotropy: Intrinsic vs. form birefringence

Polymeric macromolecular chains, by virtue of their three-dimensional architecture and the vectorial character of their covalent linkages, inherently possess polarizability anisotropy, meaning their susceptibility to electric-field-induced dipole formation varies as a function of direction [21]. At the monomeric level, this anisotropy confers orientation-dependent optical responses under defined conditions. In a completely amorphous phase, the chains adopt a stochastically disordered, isotropic distribution, resulting in a net cancellation of the anisotropic polarizability contributions emanating from individual repeat units. Macroscopically, therefore, the bulk material presents itself as optically isotropic, exhibiting no discernible birefringent signature [17].

As a representative case, within the molten rheological regime, the linear interdependence of birefringence and extensional stress is formalized through the stress-optical coefficient (C_r) [17]:

$$\Delta n = C_r \times \sigma \quad (1)$$

In the glassy state of polymers, however, a similar relationship holds, albeit with a different coefficient termed the photoelastic coefficient (C), defined as follows [17]:

$$\Delta n = C \times \sigma \quad (2)$$

In a completely amorphous phase with perfectly random chain orientation, the anisotropic polarizability contributions from individual repeat units cancel out, rendering the bulk material optically isotropic with no birefringence. However, in practice, amorphous polymers frequently exhibit birefringence due to molecular orientation and residual stresses induced during processing operations such as injection molding, extrusion, or stretching [17].

Notably, the coefficients C_r and C may exhibit disparities not only in absolute magnitude but also in their polarity (i.e., positive versus negative values) for a given polymer system [22]. This fundamental distinction underscores the profoundly different orientational mechanisms operative in the melt versus the glass. Within the molten phase, unrestricted segmental motion facilitates chain extension predominantly collinear with the applied load. In stark contrast, the glassy state, characterized by severely hindered molecular mobility, may give rise to anomalous orientation orthogonal or even antiparallel to the stress vector, or may manifest only highly localized, incipient rearrangements [23, 24]. The observed sign inversion of the relevant coefficients thus serves as a direct proxy for the disparate physical and dynamical states of the macromolecular assembly [17].

Since the operational environment for most polymeric photonic elements, including planar waveguides, refractive lenses, and functional optical films, is the glassy state, rigorous characterization and suppression of the photoelastic coefficient (C) assume paramount importance [25, 26]. This parameter dictates the sensitivity of the material's birefringent response to residual mechanical or thermal stresses, thereby directly impacting phase retardation and polarization fidelity. Optical device engineering consequently necessitates meticulous consideration of both the amplitude and algebraic sign of C to mitigate deleterious effects such as phase front distortion, depolarization, and stray interferometric artifacts. As such, C transcends its role as a mere material constant, functioning instead as a pivotal design metric in the development of advanced polymeric optics [17].

During conventional polymer forming operations, exemplified by injection molding, extrusion, and hot drawing, the material is processed in the fluid melt state. Birefringence initially developed under these

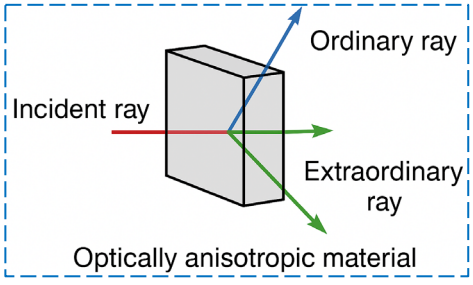

Fig. 1. Schematic representation of the birefringence phenomenon.

conditions, as governed by the stress-optical coefficient C_r, is generally transient and does not survive vitrification into the final solid product [27, 28]. This relaxation phenomenon arises because the cooling trajectory through the glass transition provides a kinetic window for chain segments to undergo partial re-randomization, effectively annulling the orientational memory of the melt state. The ultimate, steady-state birefringence in the finished optical component is influenced by multiple factors, including the glassy-state photoelastic coefficient C, residual molecular orientation retained from processing, thermal history and cooling rate, degree of crystallinity (if any), and frozen-in stresses [17].

In concise summation, birefringence in polymeric systems originates from stress- or process-induced anisotropy in macromolecular chain orientation. Within an ideal amorphous matrix, the stochastic arrangement of chains yields a macroscopically isotropic, birefringence-free medium [29]. The imposition of mechanical stress disrupts this randomness, inducing preferential alignment and the concomitant emergence of birefringence. The linear interdependencies linking stress and birefringence were formally addressed in Eqs. 1 & 2. Ultimately, a deep appreciation and deft manipulation of these optical coefficients form the bedrock upon which the reliable and high-fidelity design of polymeric photonic devices is constructed [17].

1.3. Chain orientation: Melt, glassy state, and birefringence

In the molten state, polymer chains possess substantial freedom for translational and rotational motion. When mechanical stress, such as tension or shear, is applied to the material, the molecular chains align and orient preferentially along the direction of the applied stress. This induced order imparts a transient birefringence to the material in the molten state, as the spatial distribution of chains is no longer random [30]. However, upon the onset of cooling, molecular mobility diminishes, and the chains exhibit a tendency to revert toward their equilibrium, disordered configuration. During this stage, a portion of the orientation is lost as the chains undergo relaxation and return to a state of randomness. Nevertheless, this reconfiguration is incomplete; moreover, conformational changes in the spatial arrangement of chains may also occur during cooling, which further influences the optical behavior of the material.

Upon full vitrification into the glassy state, segmental dynamics are effectively quenched, and the supramolecular architecture becomes kinetically trapped. Should any vestiges of melt-state orientation persist through the relaxation window, they become permanently enshrined within the rigid glassy matrix [31]. This remnant orientational order constitutes the source of persistent birefringence manifest in the solid polymer. Thus, in the context of polymeric photonic components, the observed steady-state birefringence is largely attributable to residual molecular anisotropy inherited from the processing melt and subsequently immobilized by the glass transition.

For polymers in the glassy state, the terminal birefringence (Δn) is often described by the relation in Eq. 3, where f is the Hermans orientation parameter (ranging from 0 for completely random orientation to 1 for perfect uniaxial alignment), and Δn^0 is the intrinsic birefringence for fully oriented chains [17]:

$$\Delta n = f \times \Delta n^0 \quad (3)$$

Within this expression, the parameter f quantifies the extent of macromolecular alignment, assuming values spanning from zero, indicative of a completely isotropic, orientationally random ensemble, to unity, corresponding to the idealized case of perfect uniaxial order [32]. The term Δn^0 designates the intrinsic birefringence, a material-specific constant representing the maximum attainable birefringence under conditions of full chain extension and collinear alignment. This foundational relation serves as the cornerstone for interpreting the optical anisotropy of glassy polymers, explicitly linking the observable birefringence to the underlying degree of molecular orientation [17].

This particular manifestation of optical anisotropy, which stems directly from the spatial registry of the polymer backbone, is formally classified as orientational birefringence. As the alignment parameter f increases, the disparity between the refractive indices along the principal orthogonal axes correspondingly intensifies [33]. The phenomenon thus provides a direct and quantifiable conduit between the microscopic architectural details, namely, chain conformation and orientational distribution, and the emergent bulk optical properties. In this regard, investigations into the orientational birefringence of polymeric materials forge an essential nexus connecting the fundamental principles of molecular physics with the pragmatic demands of optical device engineering [17].

1.4. The concept of form birefringence and its control

The intrinsic birefringence Δn^0, representing the maximum birefringence at perfect uniaxial alignment (f = 1), cannot be obtained directly from f alone. Experimentally, Δn^0 is determined by measuring birefringence (Δn) as a function of the orientation parameter f obtained from IR dichroism or polarized Raman spectroscopy and extrapolating to f = 1 using the linear relation in Eq. 3 [34]. Furthermore, X-ray diffraction (XRD) affords insight into chain registry within ordered, crystalline domains, while optical techniques, including ellipsometry and polarimetric analysis, provide alternative routes for the accurate extraction of both f and the resultant Δn^0. Collectively, these metrological approaches underpin the quantitative analysis of birefringence phenomena essential to the rational development of polymeric photonic media [17, 35].

A foundational expression central to the interpretation of orientational birefringence is presented below [17, 35]:

$$\Delta n = n\parallel - n\perp \quad (4)$$

Within this formulation, $n\parallel$ corresponds to the refractive index experienced by an optical field polarized collinear with the axis of macroscopic drawing or molecular alignment, while $n\perp$ pertains to the index encountered by the orthogonally polarized counterpart [36]. The arithmetic difference between these directional indices serves as a direct metric of the material's birefringence, encapsulating the optical asymmetry inherent to the oriented system [17, 35].

For polymer films processed via uniaxial hot-stretching protocols, the draw axis inherently defines the parallel polarization reference frame ($\parallel$). Eq. 4 thus furnishes a direct quantitative descriptor of the process-induced birefringence [37]. As the imposed extensional strain is amplified, the resulting divergence between the orthogonal refractive indices escalates commensurately, thereby augmenting the net birefringent signature. This fundamental tenet forms the operational basis for the fabrication of a wide array of functional optical films, encompassing dichroic polarizers and phase-retardation elements (wave plates) [17, 35].

In summation, the suitability of a polymeric material for photonic applications is fundamentally governed by two cardinal optical metrics: (1) the intrinsic birefringence (Δn^0), a material constant that quantifies the ultimate birefringent potential realizable under conditions of perfect uniaxial chain extension [38]. This property is intimately tied to the molecular architecture, particularly the presence and distribution of polarizable moieties such as aromatic rings or strongly dipolar functional groups [39–41]. (2) The photoelastic coefficient (C) is a parameter that captures the susceptibility of the refractive index to externally applied or residual mechanical stresses within the glassy state. Elevated values of C denote a heightened optical sensitivity to mechanical perturbation, whether from external loads or internal strain fields. Accordingly, the rational development of precision polymer optics mandates the simultaneous optimization and careful balancing of both the intrinsic structural anisotropy (Δn^0) and the extrinsic stress-optical response (C) to ensure robust and stable device functionality. A diagrammatic representation of the mechanistic origins of orientational birefringence in polymeric systems is provided in Fig. 2 [17, 35].

Form birefringence is a type of birefringence that arises not from the orientation of polymer molecular chains, but rather from the physical and geometric structure of the material at the nanometer scale [42]. This phenomenon occurs when the material possesses a periodic arrangement or pattern whose characteristic dimensions are smaller than the wavelength of light. Under such conditions, as light traverses the material, it encounters regions of differing density or refractive index, resulting in slight variations in propagation path and velocity along different directions. This disparity gives rise to an apparent birefringence whose origin is purely geometric in nature, rather than stemming from molecular anisotropy. However, because this effect does not derive from the intrinsic molecular anisotropy of the polymer, it receives comparatively less attention in fundamental analyses of polymeric optical behavior [17, 43].

In engineering and optical applications, the magnitude of birefringence in polymers must be meticulously controlled, as the performance of numerous polymeric optical devices is contingent upon it [44]. For instance, in lenses and polarizer protective films employed in liquid crystal displays (LCDs), the presence of birefringence can induce beam deviation, image distortion, or color shift; hence, its value should be minimized or ideally reduced to zero. Conversely, in materials such as retardation films utilized in LCDs for phase and polarization management, birefringence must be precisely and controllably adjusted to achieve the desired optical functionality. For this reason, understanding the nature of birefringence, whether structural (form birefringence) or molecular (orientational birefringence), is essential for the design and optimization of polymeric optical materials [17, 43, 45].

Following the established roadmap of this study, step 1 has established the foundational physics and rigorous first-principles definitions of optical birefringence (Δn). Building upon this theoretical framework, the subsequent analysis will proceed systematically through the remaining stages of the investigation: Step 2 will delve into the molecular engineering of the polymer matrix via the Lorentz–Lorenz equation to correlate molar refraction with intrinsic optical properties. Subsequently, step 3 will address the physical mechanisms of anisotropy induced by dynamic processing, followed by step 4, which examines nanocomposite synergy with a focus on interfacial chain ordering around high-aspect-ratio fillers. The roadmap culminates in step 5, exploring advanced anisotropy phenomena such as photoinduced birefringence in azobenzene-containing systems, and finally step 6, which synthesizes these findings through experimental validation and translational application outlooks. You can also see the roadmap of this article in Fig. 3.

2. Molecular design of the polymer matrix: Chemistry dictating polarizability

Broadly considered, the refractive index exhibited by polymeric materials is governed by two overarching determinants: (1) the intrinsic chemical constitution of the monomeric repeat units, and (2) the supramolecular arrangement and physical state of the assembled chains. In essence, the refractive index is governed by both the intrinsic electronic polarizability of the constituent chemical bonds and the macroscopic density of the material. Monomer architectures enriched with electron-dense atoms or substituents, exemplified by sulfur, phosphorus, and the heavier halogens, display markedly enhanced polarizability [42, 44, 46]. This augmentation in electronic polarizability translates directly into a magnified bulk refractive index. Accordingly, the strategic selection and molecular engineering of monomeric building blocks stand as a paramount consideration in the pursuit of polymeric media boasting high refractive indices and tailored photonic functionality [17].

The incorporation of conjugated frameworks and aromatic ring systems promotes extensive electron delocalization, thereby substantially boosting the material's polarizability [47]. Illustratively, monomeric units functionalized with phenyl substituents predispose the resultant polymer toward elevated refractive indices, a direct consequence of the pronounced polarizability inherent to the aromatic π-electron cloud. This observation reaffirms the profound and direct influence wielded by monomer-level chemical design over the emergent optical attributes of the polymer [17, 48].

Moreover, the specific character of the covalent linkages and the pendant groups decorating the macromolecular backbone can either facilitate or impede the field-induced distortion of the electronic envelope. Such modulations directly impact the nature of light-matter interactions, affording a versatile handle for the precise tuning of both refractive index and the broader optical signature [17].

The macroscopic density of the polymer further emerges as a pivotal parameter dictating refractive index; an increased density corresponds to a greater volumetric concentration of polarizable oscillators, thereby driving the refractive index upward [49]. The mode of chain packing, specifically, the prevalence of crystalline order versus amorphous disorder, also carries substantial weight. Processing-induced chain

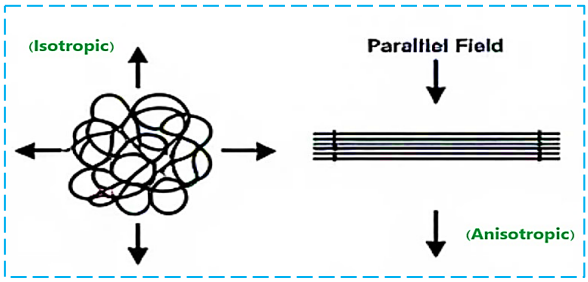

Fig. 2. Generation of orientational birefringence in polymers.

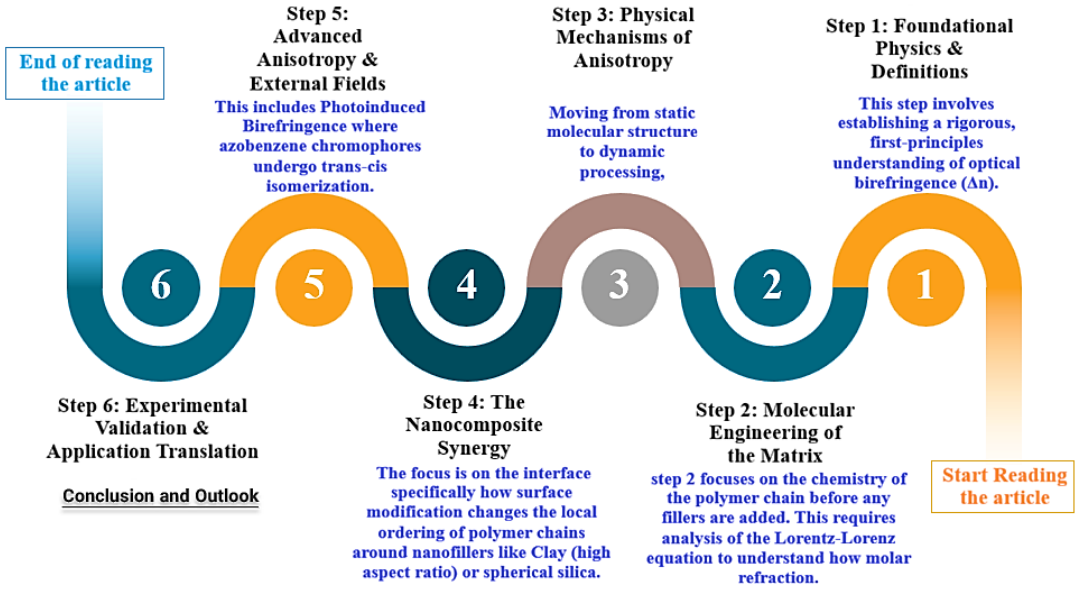

Fig. 3. The road map of this article.

orientation can impart macroscopic optical anisotropy, a condition that not only elicits birefringence but may concurrently amplify the effective refractive index measured along the axis of preferential alignment [48].

Furthermore, polymers characterized by elevated molecular weights often exhibit enhanced densification and, consequently, superior refractive indices. The inherent stiffness or segmental flexibility of the chains further dictates the attainable degree of intermolecular packing, thereby modulating the net polarizability density [48].

Within the specialized domain of high refractive index polymer (HRIP) engineering, a constellation of molecular descriptors has been empirically linked to superior optical merit. As elucidated in the previous works, polymeric architectures incorporating features such as aromatic moieties, sulfur-bearing functionalities, halogen substitution (with the notable exception of fluorine), phosphorus-centered groups, and organometallic complexes routinely exhibit augmented refractive indices [50, 51]. The integration of such substructures serves to amplify both the intrinsic electronic polarizability and the local electron density, culminating in a pronounced elevation of the bulk refractive index [43, 52].

Polymers that incorporate a high refractive index atom or functional group directly into the polymer backbone are designated as intrinsic HRIPs. Among these, sulfur-based polymers have garnered the greatest attention. These polymers have been modified with a diverse array of groups and structural motifs, including thianthrenes, thioethers, sulfones, and various other functional constituents [53]. Such modifications serve to enhance both the polarizability and the intrinsic refractive index of the polymer. In addition to backbone modification with functional groups, researchers have increasingly turned to the use of inorganic reinforcements to further augment optical properties. These inorganic additives can improve the optical characteristics, such as refractive index and thermal stability, of the polymeric matrix [17, 43].

2.1. Design parameters for high refractive index polymers (HRIPs)

A substantial body of research has established that high refractive index polymers (HRIPs) constitute indispensable materials for a diverse array of photonic applications, with the specific property requirements being contingent upon the final form factor, be it a thin film, a bulk lens, or a planar waveguide. The three predominant application domains for HRIPs encompass: thin-film coatings or interfacial layers, freestanding refractive lenses, and optical waveguide structures [17].

In the context of thin-film integration within optoelectronic platforms such as organic light-emitting diodes (OLEDs) or CCD/CMOS imaging arrays, the preferred material profile mandates exceptional optical clarity at submicron thicknesses, robust thermal endurance, and minimal birefringent signature [54, 55]. For monolithic lens elements, these criteria are further augmented by the necessity for a substantial Abbe number indicative of suppressed chromatic dispersion coupled with adequate mechanical integrity. Within guided-wave photonic architectures, HRIPs are deployed as cladding media, wherein their optical contrast relative to the core facilitates the condition of total internal reflection, thereby ensuring efficient spatial confinement of the propagating mode. Here, ultra-high transparency is paramount to attenuate propagation losses [17, 35].

The rational development of HRIPs exhibiting tailored performance hinges upon the careful consideration of four cardinal design parameters: (1) Refractive index, the fundamental metric dictating the phase velocity of light and, consequently, the degree of refraction and focusing power in lensing applications. (2) Abbe number, a measure of wavelength-dependent dispersion wherein elevated values correspond to diminished chromatic aberration and enhanced image resolution. (3) Birefringence (Δn), denoting the directional anisotropy in refractive index; as previously elaborated, its stringent regulation is imperative in

film and lens contexts to suppress optical distortion and stray depolarization effects. (4) Ancillary chemical and physical determinants, encompassing macromolecular backbone configuration, the nature and distribution of polarizable or aromatic substituents, the degree of crystallinity, process-induced chain orientation, fabrication methodology, and the incorporation of additives or nanoscale inclusions [17].

2.2. The Lorentz-Lorenz equation

A foundational tool for estimating the refractive index of polymers is the Lorentz–Lorenz equation, which relates the refractive index to molecular polarizability and molar volume. This equation is extensively employed to estimate the refractive index of polymers and relates the refractive index to the molecular properties of the polymer repeat units. The equation is expressed as follows [56, 57]:

$$\frac{n^2-1}{n^2+2}=\frac{R}{M}\rho=R_m\frac{M}{V}=\frac{R_m}{V_m} \quad (5)$$

where n is the refractive index of the polymer, R_m is the molar refraction derived from the summation of atomic and functional group polarizabilities present in the polymer structure, and V_m is the molar volume, which expresses the relationship between molecular weight and the molecular volume of the polymer unit. In other words, the refractive index of a polymer is governed by the intrinsic polarizability of its chemical constituents and its molecular packing density. This equation enables designers to predict and control the refractive index of a polymer through the judicious selection of monomers and functional groups [56, 57].

The above equation can be reformulated to calculate the refractive index n directly from R_m and V_m [56, 57]:

$$n=\sqrt{\frac{1+2\frac{R_m}{V_m}}{1-\frac{R_m}{V_m}}} \quad (6)$$

This relationship demonstrates that incorporating substituents with high molar refraction (R_m) and low molar volume (V_m) can effectively elevate the refractive index of the polymer. Stated more simply, the intelligent selection of monomers and chemical groups possessing high polarizability and compact molecular volume enables the production of polymers with high refractive indices and optimized optical properties [56, 57].

Thus, the Lorentz–Lorenz equation, as referenced in Eqs. 5 and 6, constitutes a vital tool for predicting the refractive index of polymers. In essence, this equation informs how the refractive index n of a polymer may be modulated through the strategic selection of pendant molecular groups. This selection typically entails maximizing molar refraction (R_m) while simultaneously minimizing molar volume (V_m) [57].

Stated differently, to increase the refractive index of a polymer, one must incorporate groups along the polymer backbone that exhibit high polarizability (high R_m) yet occupy a relatively small volume (low V_m). This approach enhances the degree of light bending within the material, thereby increasing the refractive index [56].

Whereas the Lorentz–Lorenz equation governs the absolute magnitude of n, the Abbe number (ν_D), introduced subsequently, characterizes the wavelength dependence of the refractive index. This property pertains to what is termed dispersion in optics. Dispersion of the refractive index gives rise to phenomena such as the separation of white light into its constituent spectral colors. Consequently, even if a material possesses a high refractive index, excessive dispersion may render it unsuitable for certain optical applications [57].

2.3. The Abbe number

The Abbe number, conventionally symbolized as ν_D, constitutes a dimensionless metric that quantifies the dispersive character of an optical medium. In essence, this parameter gauges the wavelength sensitivity of the refractive index, specifically, the degree to which n varies as a function of the incident optical frequency [58, 59]. Materials exhibiting elevated ν_D values are characterized by low dispersion, implying a nearly invariant refractive index across the visible spectral window. In contrast, diminished ν_D values are indicative of pronounced dispersion, wherein the refractive index undergoes significant modulation with changing wavelength [60].

A substantial Abbe number is critically advantageous for refractive lens elements and high-precision optical assemblies, most notably in the domain of ophthalmic and corrective eyewear, where the suppression of chromatic aberration is a primary design imperative. It is important to distinguish between refractive index (n), which determines the bending angle and optical power of a lens, and the Abbe number (ν_D), which quantifies the wavelength dependence of the refractive index (chromatic dispersion) [56, 61].

The Abbe number is formally defined by the following expression [35]:

$$\upsilon_D=\frac{n_D-1}{n_F-n_C} \quad (7)$$

In this expression, n_D designates the refractive index measured at the sodium D-line emission (589.3 nm), n_F corresponds to the index at the hydrogen F-line (486.1 nm), and n_c pertains to the hydrogen C-line (656.3 nm) [17]. Conceptually, the numerator of this relation captures the overall refractive power of the medium relative to vacuum, whereas the denominator reflects the magnitude of index variation across the visible spectrum, specifically, the dispersion between the blue and red extremities [62]. A comparatively large ν_D is thus indicative of minimal chromatic dispersion, with the refractive index exhibiting near-constancy. In contrast, a reduced ν_D value denotes substantial dispersion, wherein the index is strongly dependent upon the incident wavelength [60].

Table 1 provides a comparative compilation of Abbe numbers alongside corresponding refractive indices for a representative selection of commodity and engineering polymers. Inspection of these data reveals a general trend: enhancements in refractive index (n) are often achieved at the expense of the Abbe number (ν_D), reflecting the inherent trade-off between refractivity and chromatic dispersion in organic polymeric media [35].

The findings of Matsuda et al. demonstrated that, contrary to the conventional empirical inverse relationship between refractive index (n) and Abbe number (ν_D), it is feasible through the judicious design of chemical structure (e.g., the introduction of bulky sulfur-containing groups or aromatic rings with specific geometries) to achieve polymers that simultaneously exhibit both high refractive index and high Abbe number (low chromatic dispersion). This finding holds considerable value for the design of polymeric lenses with superior optical quality [57].

Table 1. Abbe number and refractive index values for several common polymers.

Polymer	Refractive index (n)	Abbe number (ν_D)	Ref.
Poly(methyl methacrylate) (PMMA)	1.47	57	[35]
Polycarbonate (PC)	1.58	30	[60]
Polystyrene (PS)	1.59	30	[17]
Poly(ethylene terephthalate) (PET)	1.57	32	[35]

A high numerical value of the Abbe number is critically important in lenses and other sensitive optical systems, particularly in spectacle lenses and those employed in specialized ophthalmic equipment, wherein chromatic aberration must be minimized [63]. By possessing a high ν_D, lenses can focus light with negligible chromatic dispersion while concurrently maintaining the high refractive index requisite for efficient light collection and guidance [56, 61].

It should be emphasized that the Abbe number and birefringence are two fundamentally distinct optical properties with entirely separate physical origins:

Firstly, the Abbe number is an intrinsic property dependent upon the chemical structure of the polymer. Its physical origin resides in the positioning of electronic absorption bands within the ultraviolet (UV) region. Polymers containing conjugated π-systems (such as aromatic rings) or heavy atoms (e.g., sulfur and halogens) exhibit UV absorption edges that extend closer to the visible spectrum, thereby manifesting lower Abbe numbers [64]. In contrast, simple aliphatic polymers (such as PMMA), which lack such functional groups, possess more distant UV absorptions and consequently display higher Abbe numbers. The Abbe number quantifies the extent of chromatic dispersion, that is, the magnitude of refractive index variation as a function of wavelength [17].

Birefringence (Δn) can arise from both extrinsic and intrinsic origins. Extrinsically, it is imparted during manufacturing processes such as thermal drawing, injection molding, or field-induced alignment, which create preferential chain orientation. However, when polymer chains become preferentially aligned along a specific axis due to factors such as thermal drawing, injection molding, or the application of electric/magnetic fields, birefringence emerges [65]. The underlying mechanism is as follows: parallel to the direction of chain orientation, the density of chemical bonds per unit length is greater, yielding higher polarizability and a larger refractive index ($n_\parallel$); conversely, in the perpendicular direction, the bond density is reduced. The difference between these two indices constitutes birefringence: $\Delta n = n_\parallel - n_\perp$ [56, 61].

2.4. Hybrid nanomaterials for enhanced refractive index

The genesis of high-refractive-index polymer (HRIP) systems featuring the deliberate dispersion of inorganic nanoparticles within a polymeric host can be traced to pioneering investigations reported in the early 1990s [56]. This strategic paradigm marked a watershed moment in optical materials engineering, capitalizing on the well-established volume-fraction-averaging behavior of refractive index in multi-phase composites. By integrating inorganic nanoparticulate phases of intrinsically elevated refractive index, the bulk n of the hybrid construct is appreciably enhanced, all while preserving the quintessential attributes of the polymeric continuous phase, including mechanical compliance, ease of fabrication, and low mass density. Table 2 catalogs the refractive indices of a selection of pertinent inorganic constituents [56, 66].

Illustrative nanoparticulate additives encompass titanium dioxide (TiO_2), zirconium dioxide (ZrO_2), and zinc oxide (ZnO). When homogeneously dispersed throughout the polymer matrix, these nanoscale inclusions serve to augment the composite's overall optical performance [67]. A caveat accompanying this approach, however, is the propensity for high inorganic filler loadings to compromise mechanical ductility, imparting stiffness and embrittlement to the final material. To mitigate this trade-off, deliberate enhancement of the polymeric chain flexibility may be pursued, thereby yielding a hybrid system that concurrently satisfies the dual demands of optical optimization and mechanical resilience [56, 66].

As evidenced by the data compiled in Table 2, even comparatively low weight fractions, specifically below 50 wt% of nanoparticles exhibiting $n > 2$, are capable of effecting a significant amplification of the composite's macroscopic refractive index, underscoring the efficacy of this reinforcement strategy [56].

A prominent technological deployment of hybrid nanomaterials lies in their function as encapsulating media for light-emitting diode (LED) architectures. Investigations by Chau and coworkers (2007) established that TiO_2 nanoparticles, surface-passivated with acetic acid, could be successfully dispersed directly within an epoxy host. The resultant epoxy– TiO_2 hybrid films exhibited remarkable transparency coupled with refractive indices spanning n = 2.18–2.38. This exemplar serves to underscore the viability and efficacy of nanoparticulate integration as a tangible route toward augmenting the refractive index of polymeric media [17, 43].

Notwithstanding the optical enhancements afforded by nanoparticle hybridization, the intrinsic polymerization protocol exerts an equally profound influence over the ultimate microstructure and resultant photonic response of high-refractive-index polymers (HRIPs) [68]. Specifically, even within nanocomposite formulations, the particulars of the polymerization pathway encompassing kinetic parameters (reaction rate, thermal history) and the nature of the catalytic system can markedly impact matrix density, chain orientation, and the spatial distribution of the dispersed nanoparticulate phase, thereby governing the emergent optical characteristics [17].

Table 2. Refractive index (n) values of selected inorganic compounds measured at λ = 589.3 nm (sodium D-line) and room temperature (25 °C), unless otherwise specified [17].

Inorganic compound	Refractive index (n)	Measurement conditions/notes
TiO_2 (rutile)	2.70	λ = 589.3 nm, single crystal
TiO_2 (anatase)	2.45	λ = 589.3 nm, single crystal
TiO_2 (sol-gel)	1.983	λ = 632.8 nm, thin film
ZrO_2	2.10	λ = 589.3 nm, bulk
ZrO_2 (sol-gel)	1.897	λ = 632.8 nm, thin film
ZnO	1.93	λ = 589.3 nm, bulk
ZnS	2.36	λ = 589.3 nm, bulk

Accordingly, the incorporation of high-refractive-index nanoparticulate fillers exemplified by TiO_2, ZrO_2, and ZnO into a polymeric continuum invariably elevates the bulk refractive index. Provided that these nanoscale inclusions are uniformly and isotropically dispersed, the attendant increase in n is directionally invariant, imparting negligible perturbation to the native birefringent signature of the material [35].

Conversely, any departure from ideal homogeneity manifesting as anisotropic orientation, asymmetric spatial distribution, or process-induced alignment of the nanoparticles can give rise to macroscopic optical anisotropy, thereby amplifying the differential refractive index (Δn), or birefringence. Hence, rigorous regulation of nanoparticle dispersion and orientational registry is imperative for the preservation or suppression of birefringence [69]. The influence of the polymerization methodology is further mediated by several interdependent variables: (1) the reaction kinetics and thermal profile, (2) the selection of catalyst and/or interfacial compatibilizing agents, and (3) the efficiency of mixing and the degree of nanoparticle deagglomeration achieved. These parameters can collectively promote preferential molecular orientation of either the macromolecular chains or the embedded nanoparticulates. Such induced alignment engenders directionally anisotropic refractive indices, culminating in enhanced birefringence [17, 35].

In summation, the synergistic optimization of hybrid formulation and polymerization process control affords a viable pathway toward the realization of materials that concurrently exhibit elevated refractive indices and minimal, stable birefringence, a combination of attributes indispensable for demanding photonic applications, including precision lenses, optical waveguides, and advanced LED display technologies [17, 35].

3. Physical processing and morphological development

The refractive index (denoted as n) constitutes a cornerstone parameter in material optics. As formally stipulated by the International Organization for Standardization (ISO), it is defined as the dimensionless ratio of the speed of electromagnetic wave propagation in free space (vacuum) to its corresponding phase velocity within a given material medium. This relationship is succinctly captured by Snell's Law, expressed as follows [35]:

$$n = \frac{c}{\upsilon} = \frac{\sin i}{\sin r} \tag{8}$$

Eq.8 embodies Snell's law, a foundational relation in which c signifies the speed of electromagnetic radiation in vacuo and v corresponds to the phase velocity characteristic of the medium in question. The general form of Snell's law is expressed as $n_1 \sin i = n_2 \sin r$, where n_1 and n_2 are the refractive indices of the incident and refracting media, respectively, and i and r are the angles of incidence and refraction [70]. Snell's Law articulates that the quotient of the sines of the incident and refracted angles remains invariant for a given optical boundary, a constant numerically equal to the refractive index of the denser medium. Functionally, n serves as a direct metric of the fractional reduction in light speed experienced upon traversal of the material: a more substantial n implies more pronounced refraction and a commensurately diminished phase velocity [35].

Within optically anisotropic media, exemplified by oriented polymeric films and crystalline dielectrics, the refractive index acquires a directional dependence, varying with both the propagation vector and the polarization eigenstate of the interrogating beam [71]. Accordingly, rigorous metrological practice demands explicit specification of the light propagation geometry and the polarization orientation with respect to the sample's intrinsic reference frame. This directional variability is central to the phenomenology of birefringence, as the disparity between n_e (the extraordinary index) and n_o (the ordinary index) is a direct manifestation of the material's underlying optical anisotropy [35].

When a light ray passes from vacuum (or rarefied air) into a medium such as a polymer, its velocity diminishes, and the ray trajectory is refracted or bent relative to the normal to the surface. The angle formed between the incident ray and the normal is termed the angle of incidence (i), while the angle between the refracted ray and the normal is designated the angle of refraction (r) [9]. The refractive index n is wavelength-dependent. That is, for different wavelengths, both the velocity and, consequently, the propagation path of light within the material vary. If the incident light is non-monochromatic, i.e., composed of multiple wavelengths, each spectral component undergoes refraction at a distinct angle and to a differing extent; this phenomenon is termed dispersion [35].

For this reason, precise optical measurements invariably employ a monochromatic light source to enable the determination of the refractive index at a specific, well-defined wavelength. As a standard convention, the majority of empirical refractive index data for polymers are reported at the sodium D-line (Na D-line), corresponding to a wavelength of 589.3 nm (5893 Å). This reference line ensures intercomparability of data derived from disparate sources [35].

The refracted wavefront, having negotiated the sample and prism assembly, is rendered parallel to the original incident ray and is inspected through the telescopic ocular. Determination of the refractive index is effected by systematically rotating the prism assembly until the observed field of view partitions into two distinct hemifields, one luminous, the other dark, separated by a crisp, well-defined boundary. The refractive index is then interpolated directly from a calibrated vernier scale affixed to the prism housing. This established protocol routinely yields measurement accuracies surpassing 0.01% relative error [35].

The bulk refractive index (n) of a dielectric medium exhibits a direct functional dependence on the electronic polarizability (α) of its molecular constituents. Polarizability (α) serves as a metric for the susceptibility of an atom or molecule's electron density distribution to distortion or translation under the perturbing influence of an external electromagnetic field. The conceptual bridge between this microscopic susceptibility and the macroscopic optical constant n is provided by the quantity known as molar refractivity (R_m) [35]:

$$R_m = \frac{M}{\rho}\frac{n^2 - 1}{n^2 + 2} \tag{9}$$

In this expression, M signifies the molar mass and ρ denotes the volumetric mass density of the substance. This canonical relation, attributed to Lorentz and Lorenz, furnishes the rigorous theoretical underpinning for the prediction and interpretation of polymer refractive indices from considerations of molecular structure. A kindred empirical correlation, advanced by Gladstone and Dale, offers an alternative linkage between molar refractivity ($R_{m,GD}$, $R_{m,GD} = (n - 1)/\rho \times M$) and refractive index [35]:

$$n = \sqrt{1 + \frac{R_{m,GD}}{\frac{M}{\rho}}} \tag{10}$$

Eq. 10 is widely adopted in both experimental data reduction and the computational simulation of polymeric optical properties. The term $R_{m,GD}$ effectively parameterizes the joint contributions of molecular volume and electronic polarizability to the observed n. Moreover, molar refractivity is fundamentally proportional to the molecular polarizability (α) as articulated by [35]:

$$R_m = \frac{N_A \times \alpha}{3\varepsilon_0} \tag{11}$$

Here, N_A represents Avogadro's constant (the molar count of discrete entities) and ε_0 is the vacuum permittivity. The direct proportionality between R_m and α implies that macromolecular architectures possessing enhanced intrinsic polarizability will invariably manifest elevated refractive indices. This foundational insight underpins the rational molecular engineering of both high-n polymers and materials with tailored birefringence (Δn) in oriented film geometries [35].

The frequency-dependent, or dynamic, polarizability α(ν) governs the optical response at a given excitation frequency ν under non-resonant conditions, i.e., at photon energies well removed from characteristic electronic absorption features, thereby precluding resonant promotion to excited electronic manifolds. It is formally expressed by the Kramers–Heisenberg dispersion relation [35]:

$$\alpha(\upsilon) = \frac{2}{3h}\sum_n \frac{\upsilon_{n_0}\left|\langle h_0|m|h_n\rangle\right|^2}{\upsilon_{n_0}^2 - \upsilon^2} \tag{12}$$

In this quantum-mechanical formulation, υ_{n_0} corresponds to the Bohr frequency linking the ground state (0) to an excited eigenstate (n), while m is the electric dipole moment operator mediating the transition. Eq. 12 unequivocally illustrates that the emergent optical properties of polymeric materials are inextricably tied to their molecular-level electronic structure and the corresponding facility of charge redistribution [35]. Finally, it has been demonstrated by Denbigh that molar refractivity (R_m) may be reliably decomposed into additive contributions arising from the constituent chemical bonds of the molecular framework. Complementing this bond-additivity scheme, Van Krevelen has compiled extensive tabulations of group-specific refractivity increments for a vast library of chemical functionalities. These additive constants empower the predictive computation of polymer refractive indices directly from the stoichiometric and constitutional formula of the repeat unit [35].

3.1. Stress-induced birefringence: The stress-optical law

A preliminary caveat warrants emphasis: tabulated refractive index values for a given polymer may exhibit appreciable variation among disparate reference sources. Such divergence stems from the fact that the photonic response of polymeric materials is not exclusively dictated by chemical constitution but is intimately coupled to their thermomechanical provenance. To illustrate, two nominally identical polycarbonate specimens, one configured as a uniaxially oriented thin film and the other as an isotropic injection-molded plaque, will routinely yield measurably different refractive indices. The origin of this disparity resides in process-induced macromolecular alignment, which engenders an anisotropic redistribution of electronic polarizability and a corresponding modulation of the macroscopic optical signature [72].

Accordingly, a critical conceptual demarcation must be drawn between two distinct manifestations of the refractive index: (1) the intrinsic or equilibrium refractive index, which reflects the chemical identity and molecular architecture of the polymer under well-defined reference conditions (e.g., specific wavelength, temperature, and isotropic state). (2) The apparent refractive index, a process-dependent quantity that incorporates the orientational and densification effects imparted by fabrication protocols such as extensional drawing, compressive forming, or injection molding [72].

The stress-optical coefficient (C) constitutes a pivotal metric in polymer photomechanics, encapsulating the sensitivity of the refractive index to externally imposed or residually trapped mechanical stress fields. This parameter is formally defined through the linear proportionality expressed in Eq. 13 [72]:

$$C = \frac{\Delta n}{\tau} \tag{13}$$

Within this expression, Δn quantifies the induced birefringence ($n_e - n_o$), τ signifies the true mechanical stress, and C is the stress-optical coefficient (mm^2/N), τ signifies the true mechanical stress sustained by the polymer network, and C designates the stress-optical coefficient. The dimensional unit of C is conventionally reported as square millimeters per Newton (mm^2/N), a measure that directly conveys the magnitude of birefringent response elicited per unit of imposed stress. In more accessible terms, this linear proportionality implies that materials endowed with heightened mechano-optical sensitivity manifest elevated C values. Polymeric systems featuring readily orientable backbone configurations exemplified by polystyrene and polycarbonate exhibit pronounced birefringent signatures under extensional deformation, in contrast to compliant, fully amorphous networks that may yield a comparatively muted optical reaction [72].

From a mechanistic standpoint, the imposition of mechanical stress promotes the preferential alignment of macromolecular chains, thereby engendering an anisotropic redistribution of the electron density and its associated polarizability tensor. This directional inequivalence in electronic response is the direct progenitor of the observed birefringence. Consequently, the stress-optical coefficient serves as a quantitative barometer of the molecular architecture's responsiveness to mechanical stimuli, furnishing a valuable parameter for the comprehensive characterization of opto-mechanical coupling in polymeric media [72].

The stress-optical coefficient (C) exhibits a multifactorial dependence that extends beyond the mere magnitude of the imposed mechanical stress; it is additionally governed by the intrinsic structural attributes and thermal history of the polymeric material. This coefficient is quantitatively linked to the optical configuration parameter (Δα), a material-specific metric that encapsulates the orientational polarizability anisotropy characteristic of a given polymer backbone as expressed by the following relation (Eq. 14) [72]:

$$C = \frac{2\pi\Delta\alpha(n^2+2)^2}{45kTn} \tag{14}$$

In this equation, T denotes the absolute temperature in Kelvin and k is the Boltzmann constant. The parameter Δα essentially represents the difference in polarizability of molecular segments along distinct directions of the polymer chain. Consequently, the greater the anisotropy of the molecular configuration, the larger the magnitude of C. This relationship indicates that the stress-optical coefficient exhibits an inverse dependence on temperature; that is, as temperature rises and molecular mobility increases, the regular orientation of chains

diminishes, and the optical sensitivity of the polymer to mechanical stress correspondingly decreases [72].

Birefringence, or double refraction, quantifies the disparity in refractive indices along different directions within a polymeric specimen. For an optically anisotropic material, the refractive indices along the three Cartesian axes (x, y, z) are distinct and are defined as follows [72]:

$$\Delta n_{xy} = n_x - n_y, \quad \Delta n_{xz} = n_x - n_z, \quad \Delta n_{yz} = n_y - n_z \tag{15}$$

These quantities express the degree of optical anisotropy inherent in the polymeric structure, the origin of which lies in the orientation of polymer chains or partial crystallinity. For the measurement of strain-induced birefringence, rheo-optical instruments are employed. In this methodology, the polymeric specimen is subjected to uniaxial tensile strain while monochromatic light is transmitted perpendicular to the direction of applied stress. Upon stress application, polymer chains become preferentially oriented, thereby giving rise to a differential in refractive indices. In certain polymers, this orientation may be induced by external fields, such as a flow field, or may preexist within the material, as in the case of semi-crystalline polymers that possess frozen-in anisotropy. Generally, to measure the phase difference or optical retardation between the transmitted light components, devices such as the Babinet compensator or, in more contemporary instrumentation, photoelastic modulators are utilized. From the magnitude of this retardation, the birefringence Δn is calculated, and ultimately, by dividing this value by the true stress, the stress-optical coefficient C is obtained. The experimental error associated with this method is typically less than 5%, attesting to the high precision achievable in determining the optical response of polymers to mechanical loading [72].

3.2. Influencing factors: Chemical structure and chain architecture

A synthesis of the extant literature permits the distillation of four overarching determinants that collectively orchestrate the birefringent response of polymeric systems: (1) the intrinsic chemical and electronic attributes of the molecular building blocks, (2) the macromolecular chain architecture and its spatial disposition, (3) the thermal and mechanical processing history, and (4) the presence of fillers, auxiliary additives, and the prevailing physical state of the material [17, 72].

The genesis of a polymer's optical signature resides fundamentally in the chemical identity of its monomeric repeat units. The incorporation of aromatic nuclei and extended π-conjugated frameworks substantially amplifies the average electronic polarizability, which elevates the isotropic refractive index and the directional polarizability anisotropy (Δα), with the concomitant consequence of enhanced birefringence (Δn) and an augmented stress-optical coefficient (C). In a contrasting vein, the introduction of strongly dipolar substituents exemplified by nitrile (–CN), nitro ($–NO_2$), and hydroxyl (–OH) functionalities can exert a dualistic influence on chain orientation, either promoting or frustrating alignment through a complex interplay of local electrostatic fields and hydrogen-bonding networks; the outcome is highly situational, modulated by both the immediate molecular environment and the specific character of the associative forces at play. Additionally, the molecular weight (M_w) and the corresponding chain contour length represent critical variables: extended chains afford the capacity for the genesis of expansive, coherently oriented domains; paradoxically, however, a high incidence of topological entanglements may simultaneously restrict segmental reconfiguration, thereby limiting the achievable degree of orientational order [17, 72].

The intrinsic rigidity of the polymer backbone, quantified by parameters such as chain stiffness and persistence length, exerts a profound influence over the attainable degree of optical orientation. Macromolecules characterized by elevated chain stiffness, wherein bond rotational degrees of freedom are sterically or electronically constrained, display a heightened tendency to preserve extended, ordered conformations, a condition that directly amplifies the observed birefringence (Δn). The presence of sterically demanding pendant substituents, as well as the stereochemical regularity (tacticity) of the chain, can further modulate local segmental alignment, either impeding or promoting orientational order, and may indirectly affect birefringence through their impact on the development of crystallinity. Within semi-crystalline polymeric architectures, the relative volume fraction of crystalline to amorphous phases emerges as a salient consideration, given that crystalline lamellae inherently harbor frozen-in optical anisotropy. Under such circumstances, rigorous estimation of the macroscopic refractive index (n) and birefringence (Δn) necessitates the application of optical additivity formalisms that appropriately weight the contributions of the constituent phases [17, 73].

3.3. Crystallinity and morphological impact on birefringence

Density is one of the fundamental physical properties of materials, including polymers, and expresses the mass of a substance per unit volume. This relationship is defined by the following formula [17]:

$$\rho = \frac{m}{V} \tag{16}$$

where m is the mass, and V is the volume. The density of polymers is typically reported in units of g/cm³, while in the International System of Units (SI), the unit is kg/m³. Furthermore, conventional polymers exhibit densities ranging from approximately 0.8 to 2.2 g/cm³, depending upon molecular structure, degree of crystallinity, and the presence of additives. Specific volume is, in effect, the reciprocal of density and is defined as follows [17, 72]:

$$\upsilon = \frac{1}{\rho} \tag{17}$$

This quantity represents the volume occupied by a unit mass of the material. In thermodynamic investigations and polymer processing operations (such as extrusion and molding), specific volume is of greater practical utility, as its variation with temperature and pressure facilitates the analysis of material expansion or compression. Another important parameter is specific weight, or weight density, wherein the weight per unit volume rather than mass per unit volume is considered. It is expressed by the following relationship [17, 72]:

$$D = \frac{\omega}{V} = \frac{mg}{V} = \rho g \tag{18}$$

where g is the acceleration due to gravity. In the SI system, this quantity is expressed in units of N/m³. From this definition, it follows that specific weight is directly proportional to mass density, yet exhibits a location dependence through the gravitational acceleration g. The final important parameter is relative density, or specific gravity. Relative density is a dimensionless quantity obtained from the ratio of the density of the substance to the density of water at 4 °C:

$$\rho_{rel} = \frac{\rho}{\rho_\omega} = \frac{D}{D_\omega} \tag{19}$$

A critical observation warranting emphasis is that the interrelationship between density (ρ) and birefringence (Δn) in polymeric media stems from the direct modulation of electronic polarizability (α) and optical packing fraction by the former. As articulated by the Lorentz–Lorenz formalism (Eq. 5), the refractive index (n) exhibits a nonlinear functional dependence on density; consequently, any perturbation to the bulk density or the spatial registry of macromolecular chains precipitates a measurable shift in n. Given that birefringence is defined by the directional inequivalence of the refractive index, any anisotropy, whether in local mass density or in the orientational distribution of chain segments, can serve as a progenitor of birefringent behavior. In uniaxially oriented polymers, the primary origin of birefringence is the anisotropic redistribution of molecular polarizability arising from chain alignment along the draw direction, rather than density variations. While some studies have reported minor densification along the orientation axis in certain semicrystalline systems due to closer chain packing, this effect is generally secondary compared to the dominant role of orientational polarizability anisotropy. The extent of such density changes remains system-dependent and requires direct experimental verification (e.g., via density gradient columns or X-ray scattering) on a case-by-case basis [35].

In a complementary vein, specific volume ($v=1/\rho$) and relative density (ρ_{rel}) assume considerable importance in the rational design and interpretation of optical characteristics, insofar as stress-, thermal-, or crystallization-induced volumetric excursions directly impinge upon the photonic response. The application of a mechanical stress field not only promotes orientational ordering of the macromolecular backbone but may also engender a concomitant densification (a reduction in v). These synergistic phenomena collectively amplify the resultant Δn. Conversely, an elevation in temperature or the incorporation of plasticizing agents serves to diminish both density and the degree of chain alignment, thereby attenuating the birefringent signature. In summation, density and specific volume emerge as foundational parameters that, albeit indirectly, exert a decisive and fundamental influence over the birefringent characteristics of polymers by virtue of their regulatory role over polarizability, molecular ordering, and the spatial orientation of the chain ensemble [35].

Within a homologous progression of organic substances exemplified by the alkanes and cycloalkanes, the evolution of density as a function of chain elongation (increasing repeat unit count, n) adheres to a systematic and prognosticated trajectory. At modest chain lengths, incremental addition of methylene [CH_2] units yields a pronounced augmentation in density, a reflection of the comparatively expansive interstitial free volume and attenuated intermolecular cohesion characteristic of short-chain congeners. As the chain contour length extends further and the molecular architecture approximates that of a high polymer, however, the density asymptotically saturates toward a limiting plateau. This observation implies that beyond a threshold degree of polymerization, further chain extension imparts negligible additional densification, as the spatial packing efficiency and intermolecular compaction have effectively reached a quasi-invariant state. This asymptotic paradigm furnishes a conceptual cornerstone for comprehending the density behavior of authentic polymeric materials, wherein density similarly converges to a near-constant terminal value with progressive increases in chain length and degree of polymerization [35].

From a morphological standpoint, polymers are classified into two principal categories: (1) amorphous, lacking long-range molecular order, and (2) crystalline, characterized by a regular, periodic arrangement of chains. Additionally, there exist polymers that do not fall exclusively into either category but rather occupy an intermediate state; these are termed semicrystalline. Amorphous polymers lack sufficient chain registry to generate sharp, well-defined X-ray diffraction patterns. In contrast, crystalline polymers, by virtue of their highly ordered chain packing, produce distinct diffraction signatures. Examples include polystyrene (PS), which is predominantly amorphous, and polyethylene (PE), which is largely crystalline [35].

No polymer is 100% crystalline. Within any polymeric material, two distinct regions invariably coexist: crystalline domains, wherein chains are densely packed and ordered, and amorphous domains, characterized by entangled, disordered chains. Furthermore, birefringence in semicrystalline polymers arises from the disparity in optical properties between the amorphous and crystalline regions. For this reason, the more accurate designation is "semicrystalline polymer" [35].

Within crystalline regions, chains are arranged in a more ordered and compact manner, resulting in a higher local density (ρ). Consequently, as the degree of crystallinity (x_c) increases, the overall density of the polymer rises. In most polymers, the density differential between crystalline and amorphous phases is approximately 10–15%. That is, if an amorphous region exhibits a density of 1 g/cm^3, the corresponding crystalline region will possess a density on the order of 1.13–1.15 g/cm^3. Simple, unsubstituted polymers (e.g., polyethylene), by virtue of their regular, densely packable chains, display a substantial contrast between crystalline and amorphous domains, leading to a high degree of crystallinity, which in turn engenders elevated birefringence [35].

In semicrystalline polymers, the bulk density of the material is a function of the relative proportions of the amorphous and crystalline phases. Van Krevelen proposed an empirical relationship for estimating the density of a semicrystalline polymer, expressed as follows:

$$\rho_{sc} = \rho_a (1 + 0.13 x_c) \tag{20}$$

In this expression, ρ_{sc} is the density of the semicrystalline polymer, ρ_a is the density of the amorphous phase, and x_c is the degree of crystallinity (fraction crystallinity). This equation indicates that as x_c increases, the overall polymer density rises, and for a fully crystalline polymer (x_c =1), the density will be approximately 13% greater than that of the amorphous phase [35].

An increase in the degree of crystallinity influences not only density but also amplifies the optical anisotropy arising from the enhanced order of polymer chains within crystalline domains. This optical anisotropy is directly correlated with birefringence (Δn), such that as x_c increases, Δn correspondingly rises, thereby improving the optical properties of the polymer for demanding photonic applications, including retardation films and precision lenses [35].

In summary, it may be concluded that an increase in crystallinity engenders greater chain order and a reduction in structural disorder. This enhanced order amplifies the intrinsic optical anisotropy of the chains, yielding a larger Δn. Stated simply, the denser and more crystalline the polymer, the greater the disparity in refractive index between directions parallel and perpendicular to the chain axis, and consequently, the more pronounced the birefringence. Thus, density measurement and the estimation of the degree of crystallinity constitute essential metrics for predicting and controlling the optical properties of polymeric materials [35].

4. Nanocomposite effect: Interface engineering and form birefringence

The incorporation of reinforcing fillers, most notably carbon black and precipitated silica, synergistically combined with accelerated sulfur vulcanization, constitutes a cornerstone methodology for tailoring the mechanical response profile of rubbery compounds. The inclusion of such particulate phases serves a pivotal reinforcing function, manifested through measurable improvements in a constellation of mechanical metrics: augmented hardness, elevated elastic moduli (both tensile and shear), increased energy to rupture, enhanced tear and tensile strength, and superior resistance to crack growth, cyclic fatigue, and abrasive wear. From a utilitarian perspective, reinforcement may be operationally defined as the extension of component longevity under conditions predisposing the material to failure modes such as fatigue fracture [17, 35].

Illustratively, when probing the mechanistic underpinnings linking the inherent disorder of filler networks to elastomeric reinforcement, it becomes evident that the macroscopic elastic modulus is profoundly shaped by both the spatial dispersion characteristics and the interfacial interactions between the filler particulates and the contiguous polymer matrix. Notably, conventional treatments rooted in classical continuum elasticity often prove inadequate in capturing the full complexity of the physics governing such disordered, multi-phase composites. This shortcoming necessitates the deployment of alternative, multi-scale theoretical constructs capable of resolving the intricate interplay of interactions and reinforcing phenomena that manifest across disparate length regimes [17, 35].

One may thus conclude that filler inclusions perform a dual and indispensable function, simultaneously bolstering the mechanical integrity of elastomeric matrices and modulating their emergent optical characteristics. The hydrodynamic reinforcement paradigm establishes that even the dispersion of minute spherical particulates elevates the shear modulus of the host elastomer, a consequence attributable to both the volume fraction occupied by the rigid inclusions and the modulus mismatch between the dispersed and continuous phases. When nanometric fillers are uniformly disseminated throughout the matrix, their influence extends beyond mere stiffening; they can also potentiate the local orientational ordering of macromolecular chains under the combined influences of external stress fields and process-induced flows [35].

Such perturbations to the orientational distribution and local segmental packing density directly translate into an augmented birefringent response (Δn), given that birefringence is fundamentally rooted in the directional inequivalence of the refractive index. Stated differently, nanofillers by virtue of their capacity to seed localized optical anisotropy and to intensify interfacial matrix–particle coupling exert a concurrent and synergistic influence over the mechanical and photonic property suites. The judicious specification of nanofiller identity, shape anisotropy, characteristic dimension, and loading fraction therefore emerges as a versatile and potent strategy for the precise manipulation of Δn and the broader optical behavior of oriented and semicrystalline polymeric systems [35, 74].

These intricate, hierarchically structured morphologies foster an intensified degree of chain alignment within the interphase region proximal to the filler surface. As articulated by Mullins and Tobin, the concept of the strain amplification factor provides a quantitative framework for relating the locally magnified strain experienced by the matrix in the filled state to the globally applied far-field strain [35, 74].

4.1. General role of fillers in polymer composites

Dopants function as active additive species within polymeric matrices, serving to modify or enhance the optical, electrical, mechanical, and thermal characteristics of the host polymer. In their pristine, undoped state, most polymers behave as electrical insulators, and their optical properties are largely confined to simple transparency or absorption phenomena. The introduction of dopants can modify the electronic structure of the polymer; however, the generation of free charge carriers (electrons and holes) is not universal and depends on the specific doping mechanism and conditions This modification gives rise to a range of emergent behaviors, including enhanced optical absorption, variation in refractive index, reduction of the optical bandgap energy, and improved electrical conductivity. In essence, dopants fulfill the role of "energy modulators"; by introducing new energy levels within the bandgap, they govern the optical response of the polymer, rendering it suitable for optoelectronic and photovoltaic applications [2, 6].

Dopants may be broadly classified into four principal categories: metallic, semiconducting, carbon-based, and ceramic. Metallic dopants such as silver (Ag), copper (Cu), gold (Au), or nickel (Ni) are typically incorporated into polymers in the form of nanoparticles. Owing to their surface plasmon resonance characteristics, these particulates enhance optical absorption in the visible and near-infrared spectral regions and markedly elevate the electrical conductivity of the polymer. Furthermore, their presence contributes to a reduction in the optical bandgap and facilitates improved electron transport [9]. Semiconducting dopant species exemplified by zinc oxide (ZnO), titanium dioxide (TiO_2), cadmium sulfide (CdS), and cadmium selenide (CdSe) are integrated into polymeric hosts to precisely modulate their optoelectronic architecture. These nanoscale inclusions amplify reflectance, promote optical scattering, and enhance absorption within targeted spectral windows, rendering them indispensable for applications spanning organic photovoltaics, field-effect transistors, and light-emitting diode (LED) technologies [6].

Carbonaceous dopants encompassing graphene, carbon nanotubes (CNTs), and carbon quantum dots (CQDs) represent a class of low-density, electrically conductive additives that simultaneously bolster the conductivity, mechanical resilience, and thermal endurance of the polymer matrix. Within the charge percolation framework, these carbon allotropes serve as "conductive conduits," facilitating efficient carrier transport while also enhancing the photonic response and operational lifetime of the resultant devices [2]. Ceramic dopants, including $BaTiO_3$, Al_2O_3, and ZrO_2, are predominantly deployed to impart elevated thermal stability, superior mechanical strength, and enhanced dielectric constant. Although their direct contribution to optical absorption is generally modest, they affect an increase in the refractive index and augment the electrostatic energy storage density through alterations in the local polarizability and charge distribution [2].

A comparative evaluation of dopant functionalities reveals a distinct division of roles: metallic dopants deliver the most substantial gains in optical absorption and the most pronounced bandgap narrowing; semiconducting dopants are unparalleled in their capacity to promote

charge separation and radiative recombination efficiency; carbon-based dopants provide exceptional electrical conductivity and structural reinforcement; and ceramic dopants offer unmatched thermal and dielectric stability. The strategic selection of a dopant system is thus contingent upon the targeted performance metrics: where enhanced optical yield is the primary objective, metallic and semiconducting dopants are indicated; conversely, where long-term environmental stability and mechanical durability are of chief concern, ceramic dopants are favored. In recognition of these complementary strengths, contemporary research efforts have increasingly embraced multi-component dopant formulations, seeking to harness a confluence of these desirable attributes within a single hybrid material platform [6, 56, 75].

Table 3 presents a consolidated synopsis of the salient optical, electrical, and mechanical/thermal metrics, together with the operative physical mechanisms, representative size and loading regimes, and attendant practical limitations for each dopant class. It is noteworthy that dopant inclusion can engender the formation of mid-gap electronic states or establish emergent band-like features that facilitate optical transitions at sub-bandgap energies, thereby affecting a reduction or systematic alteration of the optical bandgap (E_g). Semiconducting and complex-based dopants typically afford the most pronounced leverage over E_g modulation [76].

High-refractive-index fillers exemplified by $BaTiO_3$ and TiO_2 serve to elevate the effective refractive index of the composite medium. In contrast, plasmonic nanometals amplify the extinction coefficient (k) and, correspondingly, the absorption coefficient (α) within well-defined spectral bands. The introduction of electrically conductive additives such as graphene, carbon nanotubes, or metallic nanoparticles can increase the effective free carrier density and electrical conductivity of the composite; However, the concomitant introduction of interfacial trap states and enhanced carrier scattering mechanisms may curtail the relaxation time (τ) and degrade charge carrier mobility (μ), unless mitigated through deliberate surface passivation or compatibilization strategies. For photovoltaic or light-emitting diode (LED) applications, the selected dopant must not only fulfill its intended optoelectronic function but also satisfy stringent criteria pertaining to long-term photochemical stability, environmental resilience, and seamless integration within the designated processing paradigm, be it solvent-borne deposition or melt-state compounding [77].

Table 3. Types of dopants and their principal effects on polymer-based composites.

Dopant type	Example	Morphology /size	Optical effect	Electrical effect	Mechanical/ thermal effect	Physical mechanism	Challenges	Ref.
Metallic NPs	Ag, Au, Cu, Al	Spherical, 5–100 nm	Surface plasmon peak; enhanced absorption in visible/NIR	Localized increase in electrical conductivity; potential formation of high-current pathways	Enhanced thermal conductivity	Localized Surface Plasmon Resonance (LSPR)	Agglomeration ; surface incompatibility with matrix; oxidation (e.g., Cu)	[2]
Semiconductor NPs	TiO_2, ZnO, CdS, CdSe	3–100 nm nanocrystals	Shorter-wavelength absorption; tunable optical bandgap; enhanced UV/Vis absorption depending on E_g	Enhanced charge separation and electron/hole transfer (in PV systems)	Moderate to good thermal stability; increased surface hardness	Formation of intermediate energy levels; electron transfer from polymer to nanoparticle	Toxicity (Cd-based compounds); poor surface adhesion	[9]
Quantum dots	PbS, CdSe, perovskite QDs (quantum dots)	2–10 nm	Size-tunable absorption and emission spectra; narrow emission linewidth	Can facilitate charge transport; surface passivation is often required	Minimal mechanical effect at typical low loadings; thermal stability limited by surface ligands and core composition	Quantum confinement; size-dependent bandgap (E_g) tuning	Photo- and chemical stability; requirement for core-shell architecture for stability	[2, 9]
Carbon-based	Graphene, graphene oxide, CNTs, carbon dots	CNT: tens of nm length, few nm diameter	Scattering and absorption in visible–IR; effective absorption in specific structures	Very high electrical conductivity (graphene/CNT)	Enhanced tensile strength, stiffness, and thermal conductivity	Extended π-electron network	Difficult to achieve uniform dispersion; critical particle matrix interfacial contact.	[2]
Metal complexes	Transition-metal complexes	Molecular to nano-scale	Metal-to-ligand charge transfer	Can introduce mid-gap states; facilitates charge transport	Moderate chemical stability	Molecular charge transfer	Photo-/redox stability; solubility and compatibility	[2]

4.2. Principles of doping and light propagation

Conducting polymers (CPs) in their undoped, pristine state typically exhibit low electrical conductivity, often in the semiconducting or poorly conductive range (~10^{-10} to 10^{-5} S/cm), as their charge carriers are localized and not freely mobile. Upon doping, however, the electrical conductivity of these polymers can be dramatically enhanced, in some instances approaching values characteristic of metallic conduction. The doping process in conducting polymers differs fundamentally, from an electrochemical mechanistic standpoint, from the doping of inorganic semiconductors. In polymers, dopants typically participate in oxidation–reduction (redox) reactions with the polymer backbone, affecting charge transfer onto or from the polymer chain through electron exchange. In other words, a dopant may either extract an electron from the polymer (oxidation) or donate an electron to the polymer (reduction) [78].

In this process, if the dopant extracts an electron from the polymer, electrons are removed from the highest occupied molecular orbital (HOMO), leaving a positive charge localized on the chain. Conversely, if the dopant donates an electron to the polymer, these electrons populate the lowest unoccupied molecular orbital (LUMO), generating a negative charge. The outcome of this charge exchange is the formation of localized charge carriers in the form of polarons, bipolarons, or solitons, which constitute the primary agents of electrical conduction in doped polymers [78].

Consequently, doping not only modifies the electronic structure of the polymer but also impacts its optical characteristics, including absorption, coloration, and even birefringence, since the addition or removal of electrons alters both the polarizability and the spatial arrangement of the polymer chains. This attribute is of considerable importance in the design of optoelectronic materials and optical sensors [78].

Conducting polymers are classified, based on their band structure and ground-state configuration, into two principal categories: (1) degenerate systems and (2) non-degenerate systems. In degenerate polymers, two distinct geometric arrangements of the polymer chain possess identical ground-state energies. The classic exemplar of this class is polyacetylene. In such structures, single and double bonds alternate along the chain backbone (C=C–C–C=C). Moreover, owing to electronic symmetry, these two configurational states are energetically equivalent; consequently, a discontinuity or defect in the bond alternation pattern can propagate along the chain with minimal energetic expenditure. This mobile defect is termed a soliton, which constitutes the characteristic charge carrier of degenerate polymeric systems. In contrast, non-degenerate polymers such as polypyrrole (PPy) and polythiophene (PT) exhibit two ground state structures with distinct energies. As a result, soliton formation in these materials is energetically unfavorable, and charge carriers instead manifest as polarons or bipolarons. A polaron represents a charged electron or hole coupled to a localized lattice distortion of the chain. A bipolaron, in turn, arises from the combination of two like-charged polarons [78].

Thus, electrical conduction in doped polymers is mediated by the migration of charge carriers that arise from concurrent modifications to the electronic structure and geometric conformation of the chain. In degenerate systems, these carriers are predominantly solitons, whereas in non-degenerate systems, polarons and bipolarons assume the dominant role. The type of doping, p-type or n-type, dictates whether these carriers bear a positive or negative charge [78].

The introduction of impurities into polymers exerts a pronounced influence on their diverse characteristics, thereby expanding the scope of polymer applications across various technological domains. Through the deliberate incorporation of dopant species, select physical and optical properties of the host polymer may be controllably modulated, such that their performance in targeted applications is substantially enhanced. Numerous investigations have been conducted on a wide array of polymer–dopant combinations. By way of illustration, Wasan Al-Taa'y and coworkers demonstrated that PVC films doped with varying concentrations of zinc oxide (ZnO) nanoparticles exhibit systematic alterations in several optical parameters, including the extinction coefficient and the refractive index. The findings of this study on PVC/ZnO nanocomposites revealed that, within this specific system, the extinction coefficient, refractive index, real and imaginary components of the dielectric constant, and the high-frequency dielectric constant exhibited a direct correlation with ZnO loading fraction; in other words, as the ZnO loading fraction increases, these quantities correspondingly increase. Moreover, it was observed that the optical conductivity, following the doping process, increases with increasing photon energy [78].

Complementary investigations on poly(methyl methacrylate) (PMMA) matrices containing gold (Au) nanoparticles have established that variations in particle size and weight fraction exert a significant influence on the imaginary component of the dielectric function. Similarly, composites of poly(vinyl alcohol) (PVA) and iron (Fe) have been shown to induce measurable changes in the optical absorption coefficient. A substantial body of research has been devoted to the study of such hybrid material systems, and the collective weight of evidence indicates that the introduction of dopant impurities into polymeric hosts engenders a consistent improvement in desirable optical and physical attributes [2, 78].

When light propagates from a medium of higher refractive index into a medium of lower refractive index, a fraction of the incident light is reflected, while the remainder is transmitted across the interfacial boundary. The light that traverses the interface enters the second medium at an angle that may be calculated according to Snell's law of refraction. This law is expressed as follows [78]:

$$n_1 \sin\theta_1 = n_2 \sin\theta_2 \tag{21}$$

In this relationship, n_1 and n_2 denote the refractive indices of the higher-index medium (e.g., the core of an optical fiber) and the lower-index medium (e.g., the cladding), respectively, while θ_1 represents the angle of incidence of the light within the first medium. If the angle of incidence exceeds the critical angle, the light ceases to be transmitted into the second medium and is instead totally reflected at the boundary [78].

Thus, when Snell's law is applied at a planar interface and subsequently generalized to a two-dimensional rectangular slab waveguide geometry, that is, a configuration wherein $n_1 > n_2$, the requisite conditions for the refractive indices and the angle of incidence can be established such that light propagates exclusively within the higher-index medium, entirely devoid of losses attributable to refraction or scattering (Fig. 4) [78].

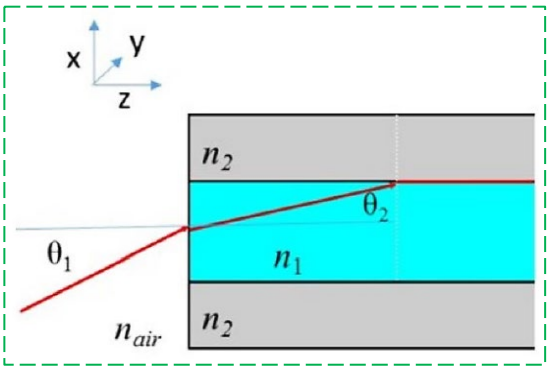

Fig. 4. Schematic representation of a slab waveguide comprising a high-refractive-index core and a lower-refractive-index cladding; light is guided within this structure via total internal reflection.

4.3. Surface modification of nanofillers

A study conducted by Inui et al. [66] focused on the surface modification of nanofillers. The central premise of this investigation was that by dispersing semiconductor nanoparticles such as ZnTe within a transparent, birefringence-free polymer matrix, it would be possible to engineer a hybrid material that simultaneously combines the advantages of the polymer (light weight, low cost, and ease of processability) with the tunable optical properties afforded by the nanoparticulate phase [66].

The principal challenges encountered in this endeavor were twofold: first, the nanoparticles exhibited a pronounced tendency toward aggregation, owing to their high specific surface area and elevated surface energy. Second, such agglomerates act as scattering centers, giving rise to undesirable light scattering and unintended birefringence. Consequently, it was necessary to modify the nanoparticle surfaces to render them compatible with the polymer matrix, thereby ensuring their uniform and stable dispersion within the host. In this study, the "hot soap" method—first introduced by Inui et al. [66] was employed. In this approach, a coordinating ligand, tri-n-octylphosphine oxide (TOPO), serves as a surface-stabilizing agent, both regulating particle growth and encapsulating the nanoparticle surface with an organic capping layer that prevents interparticle adhesion and agglomeration [66].

The resulting nanoparticles were spherical in morphology, exhibiting a mean diameter of approximately 6 nm (with some aggregates extending to ca. 20 nm), and were readily dispersible in organic solvents such as tetrahydrofuran (THF). This organic surface coating constitutes the critical enabling feature, as it permits the polymer matrix to accommodate the particulate inclusions without inducing optical scattering or birefringence. Notably, the polymer selected for this work possesses the intrinsic property of zero birefringence. This designation implies that even when the polymer is subjected to orientational processes such as molding or thermal drawing, the alignment of the macromolecular chains does not engender a directional disparity in refractive index; consequently, the polarization state of transmitted light is preserved. The overarching conclusion is that the surface modification of nanoparticles with organic ligands, such as TOPO, is the key to achieving homogeneous dispersion and suppressing the induction of birefringence [66].

The term zero birefringence signifies a condition where $\Delta n=0$ for the material. Simply put, in such a medium, light propagates with the same phase velocity irrespective of direction or polarization, and therefore, no alteration in polarization state or relative phase retardation of the wave components occurs. Under these circumstances, $n\parallel=n\perp=n_{iso}$, and the material behaves as a perfectly optically isotropic medium [66].

What, then, is the mechanistic origin of birefringence in polymeric materials? In typical scenarios, polymers manifest birefringence as a direct consequence of the orientational bias imparted to the macromolecular chains during melt processing (e.g., extrusion, injection molding) or through the application of external stress fields. Such preferential alignment engenders a directional dependence of the electronic polarizability tensor, leading to a divergence between the refractive indices measured parallel and perpendicular to the orientation axis that is $n\parallel \neq n\perp$ and the concomitant appearance of birefringence. Oriented specimens of polycarbonate or poly(ethylene terephthalate) (PET), for instance, routinely exhibit positive birefringence ($\Delta n>0$). The realization of a zero-birefringence polymer necessitates the meticulous balancing of competing molecular optical anisotropies to achieve net cancellation. This may be accomplished, for example, through the copolymerization of monomeric species characterized by birefringent contributions of opposing algebraic sign. A complementary tactic involves the strategic dispersion of nanoparticulate fillers whose intrinsic optical anisotropy is contrarian to that of the oriented polymer host. In such nanocomposite architectures, provided the filler phase is homogeneously distributed and aggregation is suppressed, the nanoparticulate inclusions can serve to offset the native birefringence of the matrix [66].

A further study, conducted by Modiri and associates [73], explored the phenomenon of laser-induced birefringence in hybrid polymer nanocomposites doped with Methyl Red, a chromophore renowned for its nonlinear optical (NLO) activity. In traditional guest–host configurations, the dye molecules are merely solubilized within the polymer continuum, lacking covalent anchorage to the matrix. This physical entrapment predisposes the system to dye aggregation at higher loadings and compromises the temporal persistence of any field-induced chromophore alignment. In marked contrast, the system under investigation featured the azo dye covalently tethered to a siloxane-based network (grafted architecture). This deliberate chemical integration effectively suppresses chromophore aggregation, substantially augments the orientational stability of the azo moieties, and markedly amplifies the magnitude and stability of the laser-induced birefringent response [73].

A complementary study by Wu et al. [79] addressed the in situ surface engineering of silver (Ag) nanofillers dispersed within an azopolymer matrix, with the express aim of fortifying the stability of photoinduced optical birefringence. The overarching goal was to achieve a homogeneous and agglomerate-free dispersion of Ag nanoparticles (NPs) within the azopolymer continuum, thereby producing a transparent, optically uniform thin film endowed with enhanced resilience against birefringent decay. While azopolymers are inherently capable of manifesting pronounced photoinduced birefringence, a persistent drawback has been the gradual erosion of this response under cyclic illumination. The introduction of Ag NPs, synthesized and passivated in situ, produced two pivotal advancements: (1) a nearly threefold amplification in the retention of induced birefringence, and (2) the unimpeded continuation of the essential trans–cis photoisomerization dynamics of the azo chromophores [79] .

The surface modification protocol hinged on the in situ thermolytic reduction of an Ag(I) precursor directly within the polymer host. Instead of dispersing pre-synthesized nanoparticles, the team employed an Ag(I) β-diketonate coordination complex readily soluble in organic media such as THF, which was molecularly blended into the polymer matrix. Subsequent thermal activation triggered the conversion of this precursor into elemental Ag nanoparticles. This synthetic strategy ensures that the nascent nanoparticles are immediately stabilized by the enveloping polymeric chains, effectively suppressing coalescence and aggregation. The resultant nanoparticles exhibited a narrow size distribution centered around 8–10 nm, and the composite films preserved their optical clarity even at substantial silver loading fractions [79].

The investigation culminated in the finding that, relative to the neat azopolymer reference, which suffered a 9.7% diminution in birefringence after five consecutive write-erase cycles, the nanohybrid analogue formulated with 5.6 wt% Ag sustained only a 2.9% reduction. This compelling disparity underscores the role of the Ag nanoparticles in modulating the local dielectric environment and engaging in specific physicochemical interactions with the azo groups, thereby dramatically bolstering the persistence of the photoinduced birefringent state. Spectroscopic interrogation via XPS and FT-IR corroborated the existence of coordination-type bonding between the silver nanoparticles and the polymer's functional moieties, with definitive evidence pointing to an interaction between silver and the nitrogen atoms of the nitrile (–C≡N) substituents [79].

5. Advanced mechanisms: External field response and tunable anisotropy

5.1. Optical anisotropy mechanisms and birefringence

The fundamental basis of optical anisotropy resides in the spatial arrangement or intrinsic structure of the constituent molecules and particles that comprise the material. In simple terms, if the molecules or particles within a medium are arranged asymmetrically or exhibit preferential alignment along a specific direction, whether induced by mechanical drawing, an applied electric field, or inherent crystalline order, light will not experience identical propagation conditions in all directions within that material. By way of illustration, in a crystal, the regular orientation of ions causes the refractive index along the x-axis to differ from that along the y-axis. In a drawn polymer, the molecular chains become aligned along the drawing axis, causing the material to transmit light more rapidly or more slowly in one direction relative to another. Thus, optical anisotropy arises from the inherent order or structural asymmetry present within the material [79, 80].

The consequence of this anisotropic or oriented structure is that the material's response to light, encompassing absorption, transmission, and phase velocity, becomes dependent upon the direction of light propagation. That is, light incident from one orientation encounters a specific refractive index, whereas light incident from an alternative orientation experiences a different refractive index. This phenomenon is termed a direction-dependent optical response. When such anisotropy is manifested at the macroscopic scale, it appears as birefringence. Accordingly, birefringence is defined as the difference between the two principal refractive indices measured along two mutually orthogonal directions within the material [79, 80].

Furthermore, as previously discussed, when light of wavelength λ impinges upon an optically anisotropic medium, the incident wavefront is resolved into two orthogonal polarization components, each experiencing a different refractive index. In the special case of uniaxial systems (such as certain oriented polymers with a single optical axis), these components are conventionally termed the ordinary ray (with direction-independent refractive index n_o) and the extraordinary ray (with direction-dependent refractive index n_e) [79, 80].

Because these two rays traverse the anisotropic medium with disparate phase velocities, they accumulate a relative phase difference at the exit interface. This accumulated path-length differential translates into a measurable phase lag, conventionally referred to as retardation. The magnitude of this retardation is mathematically expressed by the following relationship [17]:

$$\Delta\phi = 2\pi\Delta nd / \lambda \tag{22}$$

where Δϕ is the magnitude of the phase difference between the two rays, Δn is the birefringence (the differential refractive index), d is the thickness of the material, and λ is the wavelength of the incident light. This equation demonstrates that the phase retardation Δϕ is dependent upon: (1) the sample thickness (the greater the thickness, the larger Δϕ); (2) the magnitude of birefringence (Δn); and (3) the inverse of the optical wavelength (λ) [80].

In essence, optical anisotropy emerges as a direct manifestation of the directional order or structural asymmetry inherent to the material. This anisotropy engenders a directional inequivalence in the refractive index, characterized by two distinct principal values. Consequently, an incident optical wavefront bifurcates into two orthogonally polarized eigenmodes that traverse the medium at disparate phase velocities, thereby accumulating a relative phase lag (Δϕ). It is this very phase retardation that is harnessed in functional optical elements, most notably retardation films and quarter-wave plates, to precisely manipulate, compensate for, or otherwise engineer the polarization state of transmitted light [80].

5.2. Photoinduced birefringence in photochromic materials

Anisotropy arising from molecular orientation in optically or electrically active systems originates from the following principle: under normal, equilibrium conditions, the constituent molecules of a material are randomly distributed across all possible orientations; that is, they exhibit an isotropic angular distribution. However, if this random order is disrupted, whether through exposure to light or the application of an external electric field, and the molecules undergo rotation or alignment along a preferential axis, the material as a whole (at the macroscopic scale) acquires a net orientational bias. Under these circumstances, the optical response of the medium becomes dependent upon the direction of light propagation, giving rise to optical anisotropy, which may in turn manifest as birefringence [17, 81, 82].

In photochromic materials, substances whose chemical and optical properties are reversibly altered upon exposure to light irradiation with linearly polarized light induce molecular orientation. Prominent examples of such chromophores include azobenzene and its derivatives (e.g., disperse red 1, methyl red) and dithienylethene. Linearly polarized light incident upon these molecules engages in selective interactions with those chromophores whose transition dipole moments are aligned with the polarization axis, thereby effecting a gradual, macroscopic alignment of the system [17, 81, 82].

Azobenzene molecules, upon absorption of light, undergo reversible isomerization between two distinct geometric configurations: the trans (E) isomer and the cis (Z) isomer. This reversible transformation is termed photoisomerization. In the trans state, the molecule adopts an extended, rod-like, and centrosymmetric conformation. In the cis state, the molecule assumes a bent, more compact geometry. When linearly polarized light impinges upon the system, the probability of photon absorption and subsequent isomerization is a function of the angle subtended between the molecular axis and the polarization vector of the incident light. Molecules whose long axes are collinear with the polarization direction possess the highest probability of absorption and configurational change [83].

Two key processes govern this phenomenon: (1) Angular Hole Burning: Molecules oriented parallel to the polarization direction exhibit the highest absorption cross-section and are preferentially depleted from the initial trans state. Consequently, a "hole" is created in the angular distribution of the trans-state population; that is, the number density of molecules aligned along that specific direction is diminished. (2) Angular Redistribution: Molecules that have been converted to the cis state subsequently undergo thermal or photochemical relaxation back to the thermodynamically stable trans state, but this reversion occurs with a random orientational distribution, devoid of memory of the initial orientation. Through the cyclic repetition of these processes, molecules progressively accumulate in orientations orthogonal to the polarization direction of the incident light [17, 81, 82].

After numerous cycles of excitation and relaxation, the macroscopic molecular distribution becomes significantly altered, with a preponderance of molecules residing in a plane perpendicular to the polarization axis of the writing beam. This orientational redistribution engenders macroscopic optical anisotropy. The consequences of this alignment are twofold: (1) linear dichroism, the absorption of light becomes directionally dependent; and (2) birefringence, a differential refractive index emerges between two orthogonal directions, expressed as $\Delta n = n_e - n_o$, which is particularly pronounced in spectral regions where the material is transparent (e.g., the near-infrared) [83]. The kinetics and stability of this process that is, the rate at which Δn is induced and subsequently erased are contingent upon: (1) the cross-linking density of the matrix; a more rigid network restricts molecular rotational freedom, thereby impeding reorientation; and (2) the free volume within the polymer host; a larger fractional free volume facilitates greater molecular mobility and consequently yields a faster optical response [83].

Fig. 5 presents a consolidated schematic overview of the diverse mechanistic pathways that culminate in the emergence of birefringence within polymeric media. Three predominant mechanisms governing the induction of optical anisotropy and the attendant birefringent response are delineated: the electro-optic (Pockels) effect, flow- or stress-induced birefringence, and nanoparticle-mediated anisotropy. The illustration elucidates how each distinct mechanism, operating via perturbations to the molecular orientation distribution or the supramolecular architecture of the polymer host, ultimately produces a directionally dependent refractive index contrast, thereby giving rise to the phenomenon of birefringence [17, 81, 82].

In the preceding section, it was established that in photochromic systems containing azobenzene molecules, irradiation with polarized light induces a preferential orientation of the chromophores. This orientational ordering gives rise to optical anisotropy and the consequent generation of birefringence (Δn). Furthermore, the stability and kinetics of this phenomenon are governed by the intrinsic properties of the polymer matrix. This mechanism constitutes the fundamental basis for the design of numerous optical memory devices, optical switches, and photo-birefringent films [17, 81, 82].

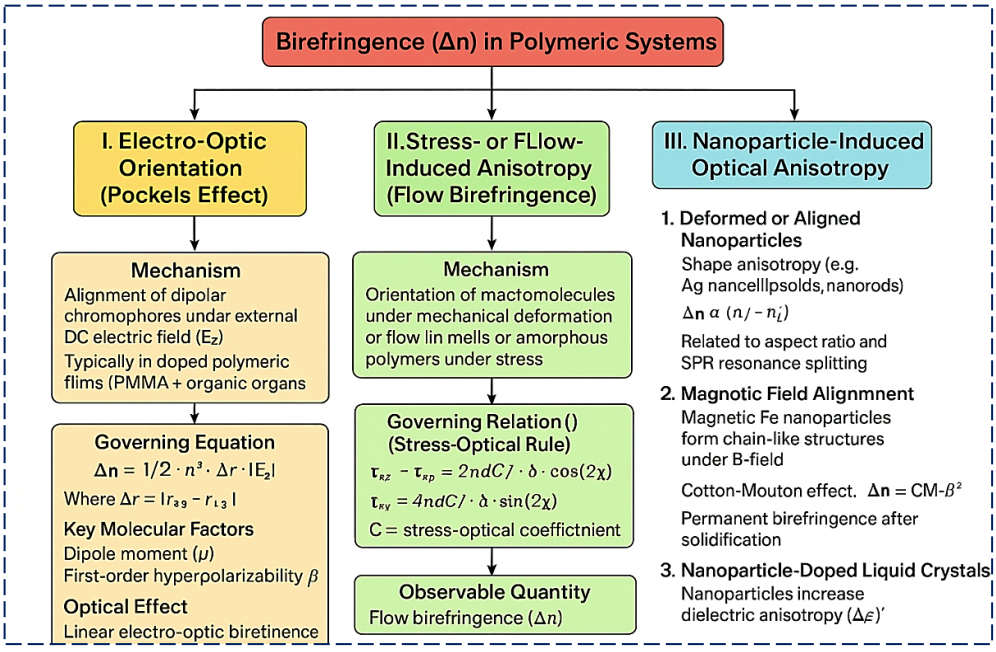

Fig. 5. Schematic representation of various optical birefringence mechanisms in polymeric systems, encompassing electro-optic, stress-optic, and nanoparticle-induced effects, with corresponding explanatory notes and governing equations for each mechanism.

5.3. Electro-Optic Orientation and the Pockels Effect

The next mechanism responsible for the generation of birefringence is electro-optic orientation, specifically the Pockels effect. In this approach, a direct current (DC) electric field is employed to induce molecular orientation within thin polymer films, particularly in systems where optically active molecules (chromophores) are dissolved or doped into a polymer matrix such as PMMA (poly(methyl methacrylate)). When an electric field is applied perpendicular to the film plane (along the z-axis), molecules possessing a permanent dipole moment undergo preferential alignment along the direction of the applied field. This process, termed poling, is typically conducted at temperatures near the glass transition temperature (T_g) to facilitate sufficient segmental mobility, after which the sample is cooled to freeze the induced orientation into the glassy matrix [82].

Once the molecules are aligned parallel to the electric field, the material loses its initially isotropic character, and the refractive indices along different spatial directions become inequivalent. Most notably, the index along the poling axis (n_z) diverges from those in the orthogonal plane (n_x, n_y). The difference between n_x and n_z constitutes the induced birefringence. The magnitude of this birefringence is governed by two principal factors: (1) the strength of the applied electric field (|Ez|), and (2) the difference in the electro-optic coefficients along the principal axes, given by $\Delta r = |r_{33} - r_{13}|$. The corresponding equation reveals that the birefringence scales linearly with the applied field; it is precisely this linear dependence that defines the Pockels effect [81, 82].

At the molecular level, the magnitude of the Pockels effect is dictated by the electronic properties of the optically active chromophores, specifically, the magnitude of the permanent molecular dipole moment (μ) and the first-order hyperpolarizability (β), which quantifies the nonlinear electronic response of the molecule to an external electric field. These microscopic parameters govern the magnitude of the macroscopic electro-optic coefficients r_{33} and r_{13}. In practice, larger values of μ and β yield a correspondingly stronger induced birefringence. Consequently, the judicious selection of dopant chromophores such as nitrobenzene derivatives, perfluorinated chromophores, or extended π-conjugated systems is of critical importance for the design of high-performance electro-optic materials [35].

5.4. Four types of nanoscale anisotropy

Optical anisotropy derived from elongated or collectively aligned nanoparticles arises when particulates of intrinsically anisotropic morphology are dispersed within a host matrix such as SiO_2 or PMMA and adopt a non-random, oriented spatial distribution. The ellipsoidal geometry of such nanoparticles endows them with directionally inequivalent optical susceptibilities along their principal axes [74, 76, 84].

Upon illumination with polarized light, the component of the electric field vector oriented along either the major or minor axis of the nanoparticle experiences enhanced absorption. This polarization-selective attenuation originates from the phenomenon of surface plasmon resonance (SPR), whose characteristic frequency is axis-dependent, shifting between the longitudinal and transverse modes of the anisotropic particle. The resulting divergence between the extraordinary and ordinary refractive indices (n_e and n_o) is thereby magnified, with the peak birefringence (Δn_{max}) exhibiting a direct dependence on the particle morphology, most notably the aspect ratio [85].

Broadly considered, this class of anisotropy is realized by embedding non-spherical, shape-anisotropic nanoparticles exemplified by silver nanoellipsoids or nanorods within an optically transparent continuum such as SiO_2 or PMMA. The geometric inequivalence of the longitudinal and transverse dimensions imparts a directional dependence to the collective electronic response of the conduction electrons. This anisotropy manifests spectroscopically as a splitting of the surface plasmon resonance (SPR), with distinct resonance wavelengths associated with excitations along the major and minor axes. Consequently, the absorption experienced by an incident optical field becomes a function of its polarization orientation relative to the nanoparticle axes [74].

To analyze the effective optical response of nanoparticle-doped composites, the classical Maxwell–Garnett equation is widely used. However, this model is strictly valid for spherical inclusions with low volume fractions ($f << 1$) and assumes that the particles are much smaller than the wavelength of light [9]:

$$\varepsilon_{eff} = \varepsilon_m \left[\frac{\varepsilon_i + 2\varepsilon_m + 2f(\varepsilon_i - \varepsilon_m)}{\varepsilon_i + 2\varepsilon_m - 2f(\varepsilon_i - \varepsilon_m)} \right] \quad (23)$$

In this expression, ε_m denotes the dielectric permittivity of the continuous matrix phase, ε_i represents the dielectric permittivity of the dispersed nanoparticulate inclusions, and f signifies the volumetric filling fraction of the nanoparticles. A direct inference from this formalism is that the resultant birefringence scales with the geometric aspect ratio of the embedded particles. As the particle morphology becomes increasingly elongated, characterized by a larger length-to-diameter ratio, the optical contrast between the principal axes is correspondingly amplified, leading to an enhanced Δn [9].

A further category of optical anisotropy is that induced by magnetic field alignment. The operative mechanism involves the exposure of a magnetorheological fluid comprising a dispersion of iron-based nanoparticles in a curable liquid matrix to an external magnetic field during the solidification or curing stage. Under these conditions, the nanoparticles experience mutual dipolar interactions that drive their organization into extended, field-parallel chain assemblies. Subsequent curing or vitrification of the matrix renders this oriented mesostructure permanent [45].

This chain-like architecture gives rise to magnetic birefringence, commonly referred to as the Cotton–Mouton effect. The magnitude of Δn can be substantial, reaching values as high as approximately 0.37 in the terahertz (THz) spectral region, and the material can function as a quarter-wave plate without the requirement of an externally applied field. When magnetic nanoparticles (e.g., Fe_3O_4 or Fe) are suspended in a fluid matrix and subjected to an external magnetic field, dipole–dipole interactions between the particles promote their self-assembly into chain-like aggregates oriented parallel to the magnetic field lines. If the matrix is subsequently solidified, this anisotropic structure is permanently locked into place, yielding persistent optical anisotropy [2].

The next form of anisotropy is anisotropy arising from nanoparticle matrix interactions. The addition of nanoparticles (e.g., ZnO, TiO_2, or SiO_2) to azobenzene-containing polymer matrices can influence the photoisomerization dynamics through mechanisms such as free volume modification or surface-mediated interactions (e.g., hydrogen bonding or dipole-dipole coupling). This enhanced molecular freedom

accelerates the trans–cis–trans photoisomerization cycle and increases the maximum photoinduced birefringence (Δn_{max}) [81].

In azobenzene-based polymers, the photoisomerization process (trans–cis–trans) is contingent upon the capacity of the azo groups to undergo rotational reorientation within the confining matrix. The incorporation of nanoparticles (e.g., ZnO, TiO_2, or SiO_2) exerts two principal effects: (1) an augmentation of the free volume in the vicinity of the polymer chains, and (2) the establishment of surface-mediated interactions such as hydrogen bonding or dipole–dipole coupling, which may lower the activation barrier for isomerization [17].

The final category of anisotropy is anisotropy in nanoparticle-doped liquid crystals. In nematic liquid crystals (LCs), the addition of gold nanoparticles (Au NPs) can enhance both the dielectric anisotropy ($\Delta\varepsilon$) and the molecular order parameter (S). This enhancement is generally attributed to the formation of nanoparticle clusters that disrupt the antiparallel dipolar pairing of the LC molecules, thereby promoting a more uniform orientational alignment. In general, for liquid crystals such as HBPCN doped with Au NPs, an increase in Δn on the order of 20–30% has been reported. The enhanced molecular order reduces phase scattering and improves the optical performance of LC-based waveguides and tunable filters [80].

6. Characterization methodologies

The phenomenon of birefringence stands as a hallmark optical signature of anisotropic condensed matter, and its precise quantification is indispensable for elucidating the photonic and structural attributes of polymeric media, thin-film architectures, and nanocomposite assemblies [27]. Fundamentally, all birefringence characterization schemes operate on the principle of detecting the differential phase velocity or, equivalently, the refractive index contrast between the two orthogonally polarized eigenmodes (n_1 and n_2) sustained by the anisotropic medium.

This velocity mismatch engenders a measurable phase lag, or retardation, between the emergent wave components, which serves as the primary observable in optical metrology. The experimental armamentarium available for probing this effect is extensive, encompassing techniques that range from straightforward visual microscopy to sophisticated spectroscopic modalities. These approaches may be conveniently partitioned into two overarching families: (1) imaging and microscopic techniques, which prioritize the spatial visualization of anisotropic textures; and (2) interferometric and spectroscopic techniques, which are geared toward the rigorous, quantitative determination of phase retardation and the wavelength-dependent behavior of Δn.

Within the imaging domain, polarized optical microscopy (POM) remains a preeminent and ubiquitous tool for discerning and characterizing the morphology and anisotropic domains present in polymer films, offering the distinct advantage of rendering the interference colors and fringe patterns generated by optical retardation directly visible. Complementary modalities, including birefringence imaging and photoelastic stress analysis, leverage CCD-based detection and digital processing to construct high-fidelity, spatially resolved maps of the Δn distribution. For enhanced quantitative rigor, interferometric methods achieve exceptional precision in refractive index differential measurement by evaluating the relative phase shift between two coherent beams that have sampled different optical path lengths.

The spectral dimension of birefringence is interrogated through spectroscopic ellipsometry and UV–Vis–NIR spectrophotometry, techniques that deconvolve the wavelength-resolved intensity and polarization state of reflected or transmitted light to recover the dispersion of the principal indices n_1 and n_2. In contexts demanding heightened sensitivity, polarimetry is enlisted to gauge minute rotations of the polarization ellipse, whereas conoscopy provides insight into the birefringent figure and optic axis orientation in bulk specimens. For stimuli-responsive materials, time-resolved methods such as electro-optic (EO) modulation and magneto-optic characterization afford the means to track the instantaneous modulation of Δn under externally applied electric or magnetic fields. In concert, this diverse methodological repertoire delivers a holistic and nuanced understanding of the genesis, magnitude, and temporal dynamics of birefringence in both conventional polymers and advanced nanohybrid systems. Table 4 provides a concise comparison of the principal birefringence characterization techniques discussed in this section, highlighting their respective advantages and limitations. The choice of a suitable technique depends on the specific requirements of the study, including sample geometry, desired precision, spectral range, and whether spatial or temporal resolution is needed.

Table 4. A concise comparison of the birefringence characterization techniques discussed, highlighting their respective advantages and limitations.

Technique	Advantages	Limitations	Ref.
Polarized optical microscopy (POM)	Direct visualization of anisotropic domains; simple operation; useful for texture and morphology analysis	Qualitative or semi-quantitative; limited to thin specimens; subjective color interpretation	[73]
Spectroscopic Ellipsometry	High precision; wavelength-resolved n and Δn; non-destructive; applicable to thin films	Complex modeling required; sensitive to surface roughness and film thickness	[80 ,79 ,61]
Interferometry	High accuracy for phase retardation; direct measurement of Δn	Requires coherent light source; sensitive to vibration and thermal drift	[79]
Polarimetry	High sensitivity; good for small birefringence values	May require complex calibration	[66 ,57 ,56]
Photoelasticity/stress analysis	Spatially resolved stress-birefringence mapping; useful for quality control	Requires transparent materials	[86]
UV–Vis–NIR spectrophotometry	Broad spectral range; good for dispersion analysis; simple setup	Limited to transmission mode	[27]
Conoscopy	Provides optic axis orientation; useful for bulk specimens	Requires bulk single crystals or uniformly oriented regions	[89]

6.1. Polarized optical microscopy (POM)

Polarized Optical Microscopy (POM) is one of the most important and widely utilized optical tools for investigating the anisotropic optical properties of materials, particularly for the examination of birefringence in polymers, liquid crystals, crystalline substances, and nanocomposites. The fundamental principle of this technique rests upon the use of polarized light, which, upon transmission through an optically anisotropic specimen, is resolved into two orthogonal components that propagate with differing velocities. This velocity or phase differential gives rise to chromatic contrast or distinct intensity variations in the resulting image, which are indicative of differences in the optical structure and molecular order of the material [73].

The principal components and operational mechanism of a POM system comprise the following elements: (1) White light source, typically a halogen lamp or LED. (2) Polarizer: a filter positioned in the incident light path that transmits only a specific orientation of the optical electric field vector, thereby generating linearly polarized light. (3) Specimen: the material under investigation (e.g., a polymer film or nanocomposite), which is situated between the two polarizers. If the material is birefringent, the transmitted light is split into two components: the ordinary ray and the extraordinary ray. (4) Analyzer: a second polarizing filter oriented at 90 ° relative to the initial polarizer (the crossed-polarizer configuration). The transmission or extinction of light through this filter depends upon the extent to which the specimen has altered the polarization state of the incident light. (5) Objective and ocular lenses employed for magnification and focusing of the image [79].

Mechanism of optical and chromatic contrast generation: When polarized light traverses a birefringent material, the two orthogonal optical components characterized by distinct refractive indices n_e (extraordinary) and n_o (ordinary) propagate with unequal phase velocities. The accumulated phase difference between these components is expressed in Eq. 22 ($\Delta\phi = 2\pi\Delta nd/\lambda$) [56], where $\Delta n = n_e - n_o$ is the magnitude of birefringence, d is the specimen thickness, and λ is the wavelength of the incident light. The accumulated phase difference gives rise to constructive or destructive interference between the two optical components, resulting in the appearance of distinct colors and intensity variations at the analyzer plane. This phenomenon constitutes the fundamental basis for the observation of characteristic interference color patterns in POM [56, 57, 66].

POM is a powerful technique for investigating a range of phenomena, including: the degree of molecular order in polymers and drawn films; the analysis of phase behavior in liquid crystals (enabling the identification of nematic, smectic, and other mesophases); the determination of chain orientation in oriented polymers; the observation of structural evolution during mechanical drawing, thermal treatment, or the application of electric and magnetic fields; and the study of texture and morphology in birefringent nanocomposites. POM is distinguished by several notable attributes: high sensitivity to minute variations in birefringence, with reported detection limits on the order of 10^{-4} or less under optimized conditions; the capability for in situ observation of specimen behavior under dynamic thermal or mechanical conditions; minimal requirements for sample preparation; and the provision of rapid, qualitative information derived from the observed interference colors or brightness patterns [56, 57, 66].

Takahashi et al. [86] conducted an investigation into the coupled mechanical and optical responses of a polyelectrolyte hydrogel system (PDMAPAA-Q). Their central aim was to unravel the mechanistic origins of two simultaneous mechanical instabilities that arise during the rapid imbibition of water by the gel. The phenomena in question are: (1) the development of a saddle-like flexural deformation, driven by a radial gradient in the swelling kinetics between the disk periphery and its core; and (2) the onset of surface creasing, a consequence of the pronounced strain mismatch between the rapidly expanding superficial layer and the comparatively restrained interior [86].

A key finding of this work was the observation that under rapid swelling protocols, these two instabilities emerge concurrently and are dynamically coupled; the global saddle-like curvature of the gel body modulates the local creasing morphology, while the crease pattern, in turn, feeds back upon the macroscopic strain distribution. The synergistic product of this coupling is a distinctive stripe-like crease pattern, characterized by a crossed, orthogonal arrangement on the opposing faces of the gel disk, a stark departure from the more conventional isotropic, polygonal crease networks observed in uncoupled systems [86].

The investigators traced the genesis of this behavior to the field-induced alignment of rigid-rod PBDT (polybenzodithiazole) macromolecules dispersed within the hydrogel network. The inhomogeneous and anisotropic stress landscape generated by the combined saddle bending and differential swelling promotes the preferential orientation of these stiff inclusions along the local principal stress trajectories. In the saddle region, the coexistence of a compressive axis and an orthogonal tensile axis drives the PBDT molecules to adopt a bidirectional, cross-aligned configuration. This mutually orthogonal molecular alignment imparts pronounced optical anisotropy to the gel surfaces, manifesting as measurable birefringence. Notably, this crossed orientational registry in the top and bottom layers of the gel is rendered permanent upon desiccation, owing to the formation of stabilizing polyion complexes, thereby yielding a robust, kinetically trapped birefringent architecture [86].

In Fig. 6, a birefringent crystal is positioned between two polarizers whose transmission axes are oriented perpendicular to one another. White light enters the polarizer on the left, and only that component whose vibration direction coincides with the orientation indicated by the adjacent arrow is transmitted. For simplicity of representation, this light is depicted as a sinusoidal "red" wave [86].

Upon entering the anisotropic crystal, this polarized light is resolved into two orthogonal components: one vibrating parallel to a principal crystallographic axis, and the other vibrating perpendicular to the first axis. These two waves are typically rendered in distinct colors (e.g., blue and red) to facilitate their visual differentiation. The origin of this splitting lies in the differential propagation velocities of light along inequivalent directions within the anisotropic medium, a quantity proportional to $\Delta n \times t$, where Δn is the birefringence, the difference in refractive index between the ordinary and extraordinary rays, and t is the thickness of the crystal. These two emergent waves subsequently impinge upon the analyzer, which transmits only the component of light that is parallel to its own polarization axis. Consequently, the observed light intensity is a function of the phase difference, or retardation, accumulated between the two rays during their transit through the crystal [86].

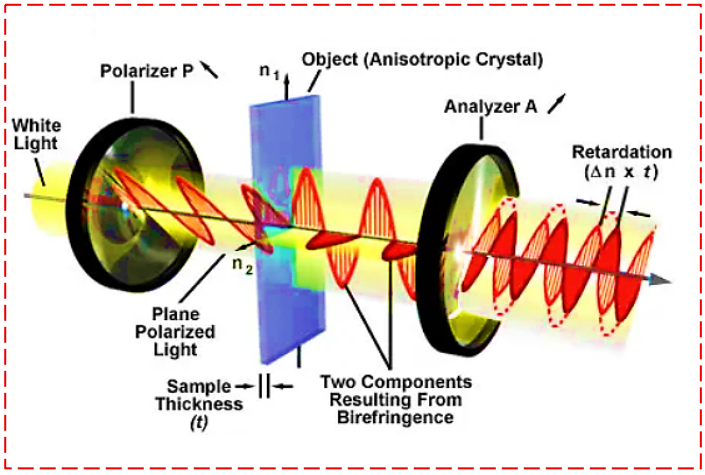

Fig. 6. Transmission of polarized light through a birefringent crystal positioned between crossed polarizers. White light, upon exiting the polarizer, is resolved into two orthogonally vibrating components within the crystal; the phase difference between these components is given by Δn × t.

6.2. Birefringence imaging and mapping

Birefringence imaging is one of the key optical methodologies for investigating the optical anisotropy of materials. This technique is predicated upon the phenomenon of birefringence, the disparity in refractive index experienced by two orthogonally polarized components of light. When linearly polarized light traverses a birefringent material, its orthogonal components propagate with differing velocities, resulting in the accumulation of a phase difference, or retardation, between them. In birefringence imaging, this phase difference is recorded at each point across the specimen as a two-dimensional spatial map, which reveals the magnitude, orientation, and character of birefringence at every location. In essence, this technique elucidates the spatial distribution of molecular orientation or photoelastic strain within the material [79, 80].

A birefringence imaging system comprises several integral components: a polarized light source frequently white light or a laser with controlled polarization; crossed polarizers (a polarizer and an analyzer), which convert the phase retardation induced by birefringence into observable variations in optical intensity; a wave plate or compensator, employed to enhance phase sensitivity and to determine the orientation of the fast and slow axes; and a CCD or CMOS camera sensitive to intensity and color, which captures the spatially resolved optical signal emanating from each pixel [61, 79, 80].

By analyzing the optical intensity at each pixel utilizing formalisms such as the Michelson interference equations or Jones matrix calculus, the magnitude of birefringence (Δn) and the orientation of the optic axis can be quantitatively extracted at every spatial location. However, these approaches rely on specific assumptions: Michelson interferometry assumes a homogeneous, weakly absorbing sample with minimal scattering and requires mechanical stability for precise phase measurement [61, 79, 80].

Wang et al. [87] have introduced an innovative snapshot birefringence imaging modality capable of simultaneous multi-wavelength operation. The primary aim of this development is the accurate and expeditious quantification of the two cardinal birefringence metrics, retardance and fast-axis azimuthal orientation within optically transparent media, most notably polymeric materials [87].

Traditional polarization-resolved imaging schemes predominantly rely on linearly polarized illumination, a configuration that exhibits no sensitivity to circularly polarized components of the transmitted field. This insensitivity constitutes an information gap, as certain birefringent signatures are incompletely characterized. To surmount this limitation, the authors implemented circularly polarized incident light. Their experimental arrangement incorporated an RGB-LED source providing three discrete spectral channels: blue (463 nm), green (533 nm), and red (629 nm). The emitted light was conditioned by passage through a circular polarizer, yielding a circularly polarized probe beam. This beam was then directed onto the birefringent specimen exemplified by polymer films or PMMA test pieces, and the transmitted optical field was registered by a color polarization camera [87].

The camera utilized in this system featured a color CMOS sensor with a resolution of 5 megapixels (2448×2048), capable of simultaneously recording four distinct polarization angles, 0 °, 45 °, 90 °, and 135 ° within a single frame. Each pixel of the sensor is dedicated to one of these four polarization orientations. From each acquired image, the three principal Stokes parameters (S_0, S_1, S_2) were extracted for each of the RGB wavelengths. Leveraging these data, the system software concurrently computes the retardance and the fast-axis azimuth angle across the entire field of view [87].

As illustrated in Fig. 7a, the optical components of the system are depicted schematically. Light is emitted from an RGB-LED source encompassing three principal wavelengths. This light is directed through a circular polarizer, which is constructed from the combination of a linear polarizer and an achromatic polymeric quarter-wave plate. The resulting circularly polarized light is then incident upon the specimen surface, where a portion of the transmitted light undergoes a phase alteration attributable to the birefringence of the sample. These modifications in phase and polarization state are registered by the color polarization camera. In Fig. 7b, the actual experimental apparatus is shown. The color polarization camera is capable of simultaneously acquiring polarization information at four discrete angles for each color channel [87].

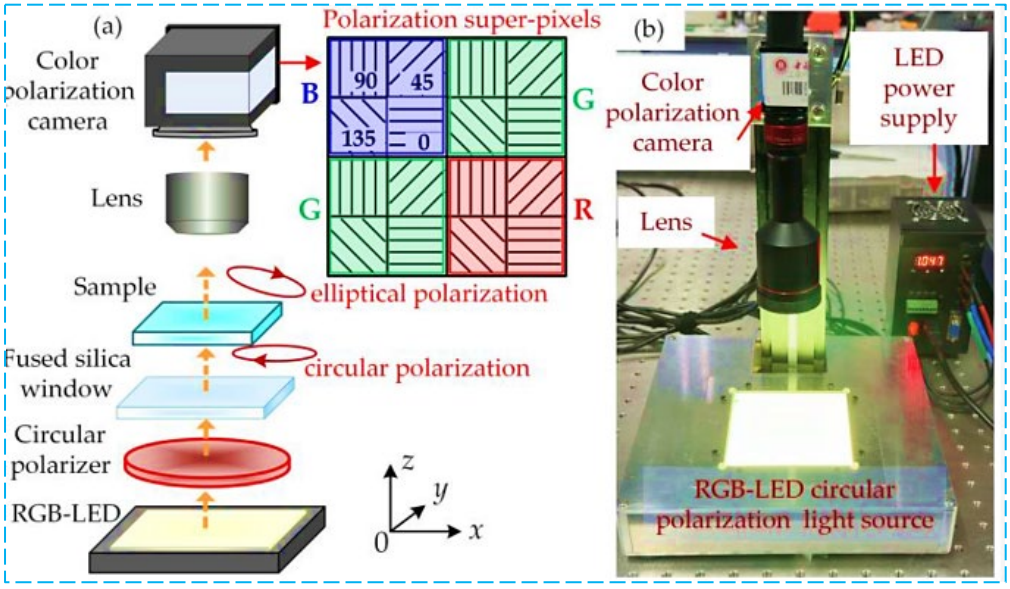

Fig. 7. Snapshot multi-wavelength birefringence imaging system. (a) Schematic representation of the optical path, wherein polychromatic light from an RGB-LED source is transmitted through a circular polarizer to generate circularly polarized illumination, which is subsequently directed onto the specimen. (b) Photograph of the actual instrument and its optical components, including the color polarization camera, telecentric lens, and protective glass stage for specimen mounting [87].

The imaging lens employed ensures a uniform, distortion-free field of view across the entire image plane. A fused silica window positioned beneath the specimen serves both a protective function and an optical alignment role, preventing direct contact between the sample and the polarizer while providing a uniform reference surface for measurement. This optical configuration has been designed with due consideration of the spectral response characteristics of both the camera and the LED sources, such that the relative intensities of the three RGB channels are optimized, and spectral errors in the calculation of the Stokes parameters are minimized [87].

To assess the accuracy of this system, an authentic polymeric quarter-wave plate was initially employed as a calibration standard to validate the measurement methodology. Subsequently, the researchers measured stress-induced birefringence in an arc-shaped PMMA specimen, both prior to and following the application of mechanical force. The results demonstrated a retardance repeatability better than 0.67 nm. Thus, the proposed method enables high-precision, multi-wavelength birefringence imaging to be performed in a single snapshot acquisition, a capability of considerable value for the optical characterization of polymeric materials and nanophotonic systems [87].

In another investigation, Honda and coworkers (2018) aimed to achieve precise measurement of birefringence (Δn) in natural silk fibers with high spatial resolution (1 μm). In this work, the researchers employed Polarized Light Imaging Microscopy augmented with a phase-controlled Liquid Crystal Retarder, thereby enabling quantitative birefringence imaging. This hybrid methodology offers exceptionally high precision and is capable of detecting minute variations in optical phase across the visible spectral range (λ = 425–625 nm) [88].

In this study, the slow axis of the silk fiber was aligned parallel to the slow axis of the liquid crystal cell to minimize phase errors. Through analysis of the transmitted intensity data and direct fitting of the optical transmission curve, a birefringence value of $\Delta n \approx 1.63 \times 10^{-2}$ was determined with an accuracy of approximately 2%. This value reflects the substantial optical anisotropy of the silk fiber arising from its molecular orientation. Owing to the relatively large thickness of the specimen, the researchers employed four discrete wavelengths to circumvent ambiguities associated with multiple-wavelength path effects. This approach enabled the accurate determination of the true Δn for thicker samples, where the accumulated phase difference may exceed multiples of 2π and would otherwise introduce discontinuities in the data [88].

To accomplish this objective, the researchers designed a simple yet highly precise optical system, as illustrated in Fig. 8, comprising the following components: (1) a white light source equipped with a narrow bandpass filter (10 nm bandwidth) for the selection of specific wavelengths; (2) crossed polarizer and analyzer for the generation and analysis of polarized light; (3) a liquid crystal cell for precise phase control and compensation of optical retardance across different wavelengths; and (4) a CCD camera for capturing the transmitted optical intensity at various angular orientations θ between the polarizer and analyzer [88].

Utilizing this methodology, the research team demonstrated that an imaging polariscope system could be constructed from relatively inexpensive components, yet deliver performance comparable to that of costly commercial instruments. A further significant advantage is the capability for high-resolution imaging at multiple wavelengths, which is critically important for the investigation of materials exhibiting spatial optical anisotropy, such as silk fibers, liquid crystals, or oriented, drawn polymers. The findings revealed that brown silk (Antheraea pernyi) possesses substantial birefringence, which is directly correlated with the regular orientation of fibroin molecules along the fiber axis. This elevated value of Δn positions silk as a promising bio-derived material with tunable optical properties, meriting consideration for the design of bio-optical elements and retardation films [88].

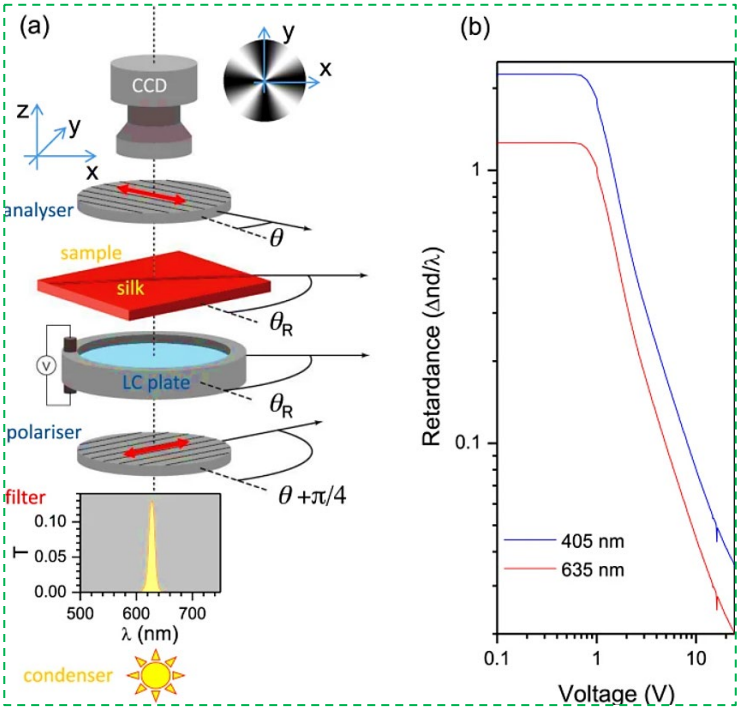

Fig. 8. Schematic of the birefringence imaging system employing polarized optical microscopy (POM) integrated with a liquid crystal (LC) phase retarder. a) Optical layout depicting the light source, narrow bandpass filter (10 nm), polarizer, silk specimen, LC cell, and analyzer. The Maltese cross pattern observed near the CCD detector results from the variation in transmitted light intensity as a function of the angular offset between polarizer and analyzer. b) Calibrated retardance versus applied voltage for the LC cell at two distinct wavelengths [88].

6.3. Interferometry and phase comparison

Another method for determining birefringence is interferometry. In this approach, the birefringence of a material is obtained by comparing the phase of two coherent optical beams. Interferometry is fundamentally based upon the comparison of the phase difference between two coherent light waves that have traversed distinct optical paths. In general, when two coherent beams are recombined after propagating along different trajectories, a pattern of bright and dark fringes corresponding to constructive and destructive interference is produced. If one of the optical paths incorporates a birefringent specimen, the phase difference between the two waves is altered, as the phase velocity along that path varies in accordance with the refractive index (which, in a birefringent medium, differs for the two orthogonal polarization components). Thus, by measuring the interferometric phase shift, the differential refractive index, $\Delta n = n_e - n_o$, can be calculated [85].

Consider light of wavelength λ incident upon a birefringent material. Within such a medium, the light is resolved into two orthogonal linearly polarized components: the ordinary component, characterized by refractive index n_o, and the extraordinary component, characterized by refractive index n_e. These two components propagate with disparate phase velocities, and upon emerging from the specimen, a phase difference (Δφ) is accumulated between them. This phase difference is expressed by the following relation [85]:

$$\Delta\phi = \frac{2\pi}{\lambda}(n_e - n_0)d = \frac{2\pi}{\lambda}\Delta nd \tag{24}$$

Within an optical interferometer, a coherent light source, typically a laser, is divided into two distinct beams. One of these beams propagates along a reference arm that remains unobstructed, whereas the second beam is directed through the sample arm, which houses the birefringent medium. Upon recombination of the two beams at the detection plane, an interference fringe pattern is formed. The resulting irradiance distribution at any point in the interference field is described by the following expression [85]:

$$I = I_1 + I_2 + 2\sqrt{I_1 I_2}\cos(\Delta\phi) \tag{25}$$

where Δϕ is the phase difference arising from birefringence.

By measuring the displacement of the interference fringes (fringe shift), the magnitude of the phase difference can be determined. However, the relationship between fringe displacement (Δm) and the birefringence-induced phase difference (Δφ) is not universal; it depends critically on the interferometer design and optical path geometry. In general, a fringe displacement of Δm fringes corresponds to a phase difference Δϕ according to the following relation:

$$\Delta\phi = 2\pi\Delta m \tag{26}$$

$$\Delta n = \frac{\Delta m\lambda}{d} \tag{27}$$

Thus, provided that the number of displaced fringes (Δm) and the specimen thickness (d) are known, the birefringence can be directly determined. The interferometric methods most commonly employed for birefringence measurement include the Michelson

interferometer, the Mach–Zehnder interferometer, and the Fizeau interferometer [85].

(a) Michelson interferometer:

In this configuration, a laser beam is divided by a beam splitter into two interferometric arms: one arm contains the birefringent specimen, while the other serves as the reference path. At the detector plane, an interference fringe pattern is observed, and the displacement of the fringes relative to the specimen-free condition directly yields Δφ [60].

(b) Mach–Zehnder interferometer:

In this arrangement, the two beams are spatially separated along completely distinct optical paths and are subsequently recombined at the output. Owing to the complete physical separation of the two arms, this configuration is particularly well-suited for the precise measurement of thicker specimens or those possessing specialized geometries [60].

(c) Fizeau interferometer:

In this method, the phase difference between two waves reflected from two surfaces, for example, the upper and lower surfaces of the specimen, is measured. This approach is extensively utilized for the characterization of birefringent thin films, as it offers exceptionally high sensitivity [60].

6.4. Spectroscopic ellipsometry

Spectroscopic ellipsometry is a non-destructive and highly precise method for measuring the refractive index (n) and extinction coefficient (k) of thin films, and from these quantities, for determining birefringence, film thickness, and optical dispersion across a range of wavelengths. This technique is predicated upon the analysis of the polarization state of reflected light. When polarized light is incident upon the surface of a material or a thin film, the s- and p-polarized components, oriented perpendicular and parallel to the plane of incidence, respectively, undergo differential reflection. Consequently, a phase difference (Δ) and an amplitude ratio alteration (Ψ) are introduced between these two orthogonal components [89].

Spectroscopic ellipsometry precisely measures these two parameters, Ψ and Δ. These quantities encapsulate the complete information necessary for the extraction of the real part of the refractive index (n), the absorption or extinction coefficient (k), the layer thickness (d), and even the degree of optical anisotropy. The operational procedure is as follows: a broadband (or spectral) light source illuminates the specimen. A polarizer defines the incident polarization state. The light reflected from the surface or transmitted through the film subsequently passes through an analyzer, and a detector records the light intensity as a function of angle and wavelength. By scanning across a range of wavelengths, the spectral curves Ψ(λ) and Δ(λ) are acquired. Finally, through optical modeling of these curves employing appropriate dispersion models such as Cauchy or Tauc–Lorentz layer formalisms, the n and k values for each layer can be quantitatively determined [89].

For optically anisotropic media exemplified by uniaxially oriented polymer films or nanohybrid assemblies, spectroscopic ellipsometry affords the distinct advantage of independently resolving n_e (the extraordinary index) and n_o (the ordinary index). The arithmetic difference between these directional indices, $\Delta n = n_e - n_o$, provides a direct and accurate quantification of the material's birefringence. The technique routinely achieves measurement precisions approaching 10^{-4} in refractive index units and is, accordingly, a cornerstone methodology in the investigation of birefringent phenomena within polymeric thin-film systems [89].

The origins of such anisotropy are diverse, encompassing intrinsic crystallographic symmetries (e.g., layered van der Waals crystals or uniaxial dielectrics) as well as process-induced molecular alignment (characteristic of oriented polymers, stretched films, and liquid crystalline phases). When a polarized optical field interacts with an anisotropic specimen, the resulting modification of the polarization state is not limited to simple amplitude attenuation or phase retardation; rather, it may involve coupling between linear and circular polarization eigenmodes, necessitating a more comprehensive mathematical description. Recognizing the limitations of standard ellipsometry in capturing this full complexity, the field has advanced toward Mueller-Matrix Ellipsometry, a formalism capable of completely characterizing the polarization transfer function of anisotropic and depolarizing samples. Spectroscopic Ellipsometry (SE) operates by quantifying the polarization alteration, whether in reflection or transmission, and conventionally expresses this change through two principal ellipsometric parameters [89]:

$$\tan(\Psi) = \frac{|R_p|}{|R_s|}, \quad \Delta = \delta_p - \delta_s \tag{28}$$

where R_p and R_s are the reflection coefficients for the components parallel and perpendicular to the plane of incidence, respectively. Ψ represents the amplitude ratio of the reflected components, and Δ denotes the phase difference between them. However, this conventional formalism is strictly applicable only to isotropic materials or those exhibiting relatively simple optical behavior [89].

In Mueller-Matrix Ellipsometry, by contrast, the complete transformation of the polarization state of light is measured. Both the incident and emergent light are represented as Stokes vectors, expressed as follows:

$$S_{out} = M.S_{in} \tag{29}$$

where M is a 4×4 matrix known as the Mueller matrix. Each element of this matrix encodes information regarding the manner in which the specimen influences the intensity and polarization state of the incident light. The diagonal elements are indicative of overall attenuation or transmitted intensity, while the off-diagonal elements are associated with transformations of the polarization state, most notably, those arising from birefringence and depolarization phenomena [60].

In Mueller-matrix spectroscopic ellipsometry (MMSE), one obtains not merely intensity variations, but the complete suite of polarization modifications, encompassing rotation of the polarization plane, changes in ellipticity, and alterations in the azimuthal orientation of the polarization ellipse. This comprehensive characterization renders MMSE exceptionally well-suited for the investigation of a broad spectrum of complex materials, including birefringent polymer films, liquid crystalline layers, nanocomposites exhibiting molecular orientation, and two-dimensional materials with intrinsic optical anisotropy such as MoS_2 or anisotropic graphene derivatives [60].

Fig. 9 illustrates the optical path in an ellipsometric system. In this configuration, a monochromatic or broadband light source initially provides illumination. The light is directed through a polarizer to establish a well-defined polarization state. The beam is then incident upon the sample surface at an oblique angle (φ). Following reflection from the specimen, the light passes through an analyzer, which interrogates the polarization state of the emergent beam. A detector

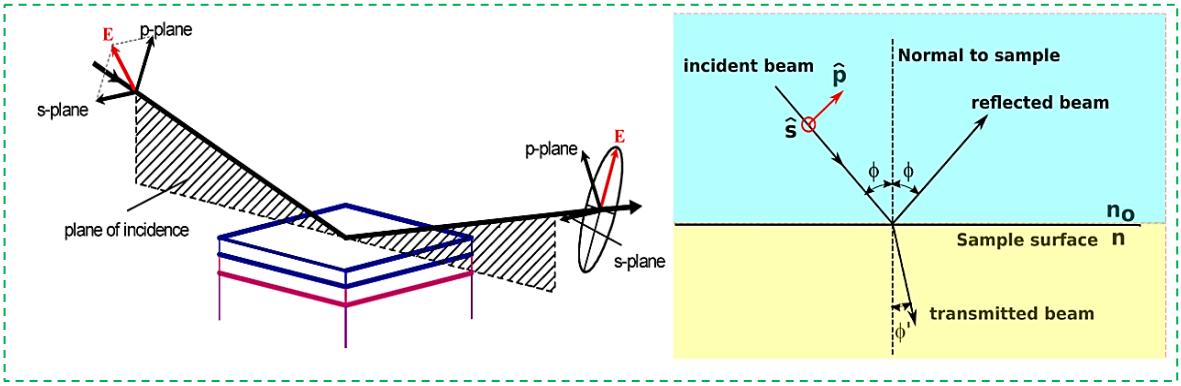

Fig. 9. Left: Schematic of a spectroscopic ellipsometry system configured for Mueller matrix measurement (MMSE). Right: Schematic depiction of a monochromatic polarized light beam interacting with a material medium, approaching from an angle designated by ϕ in an ambient air environment.

subsequently measures the intensity of the reflected components, enabling the extraction of Ψ, Δ, and the Mueller matrix. In certain system configurations, a compensator (phase retarder) is additionally positioned before the sample to facilitate more precise measurement of phase variations [89].

In another investigation, Lindsay et al. [90] conducted research on the precise measurement of birefringence using off-axis transmission ellipsometry. In conventional ellipsometric techniques, light impinges upon the sample surface at a specific angle, and through analysis of the phase and amplitude changes of the reflected or transmitted p- and s-polarized components, the optical parameters of the material, such as refractive index, absorption, and birefringence, can be determined. This study, however, examined a particular variant: the measurement of birefringence in uniaxial materials utilizing transmitted light at oblique (off-normal) incidence [90].

7. Applications

Birefringence in polymers and polymeric nanocomposites not only constitutes one of their key optical characteristics but also provides a powerful platform for the development of a new generation of optical and intelligent systems. The inherently tunable nature of polymer molecular architecture, coupled with the nanoscale engineering of fillers (nanofillers) exhibiting diverse morphologies and symmetries, affords precise control over the differential refractive index along distinct spatial directions. This attribute has positioned birefringent polymers in a pivotal role, spanning applications from retardation films employed in liquid crystal displays (LCDs) to optical sensors, stress analysis systems, and smart materials responsive to external stimuli [2, 45].

Particularly in polymeric nanocomposites, the interplay between the polymer matrix and the dispersed nanoparticles can enable the manipulation and engineering of birefringence through mechanisms such as chain orientation, the induction of optical anisotropy, and the modulation of light polarization. Consequently, in recent years, the focus of research has shifted from the mere investigation of the molecular origins of birefringence toward its functional exploitation in emerging optical technologies, flexible displays, magnetic and thermal field sensors, and the design of intelligent photonic materials [13].

The application of birefringence in polymeric display technology encompasses viewing angle compensation, image quality enhancement, and the minimization of birefringence to suppress undesirable optical artifacts. In display technologies, a principal challenge is the variation in color and the degradation of contrast when the screen is observed from oblique viewing angles. This issue predominantly arises from the anisotropic behavior of light within the various layers of the display, particularly in liquid crystal displays (LCDs). To address this challenge, birefringent polymer films with precisely controlled optical anisotropy are employed, which are capable of modulating the phase and polarization orientation of the transmitted optical wave. Through careful engineering of the refractive index contrast between the principal axes (n_1 and n_2), these films can balance the angular distribution of polarized light, thereby expanding the effective viewing angle of the display. However, effective compensation requires precise design of several birefringence parameters. In this context, birefringence functions not as a defect, but as a deliberately designed optical tool for correcting the trajectory and polarization state of light rays. Successful implementations of this strategy are exemplified by quarter-wave retardation films and viewing angle compensation films utilized in LCDs, which are fabricated as thin polymeric layers possessing a specific molecular orientation [35, 82].

A further key application of birefringence in polymeric display technology is the enhancement of image quality with respect to resolution, contrast, and luminance uniformity. In liquid crystal displays, precise control over the polarization state of light transmitted through each pixel is critically important, as even minor inhomogeneities in the orientation of polymer molecules or variations in the refractive index can induce color distortion or degrade image sharpness. Through the meticulous engineering of birefringence in the constituent polymeric layers, both the optical path and the accumulated phase difference can be tailored such that the emergent light exhibits uniform behavior across a range of viewing angles and intensities. For instance, the deployment of oriented polycarbonate or stretched polyester films as phase-controlling elements promotes a stable polarization state and mitigates unwanted reflections at internal layer interfaces [91].

Fig. 10 provides a schematic visualization of how birefringence is harnessed within polymeric display media. The illustration maps the propagation of light through the stratified polymer film stack, indicates the preferential alignment of the macromolecular chains, and depicts the resultant modulation of the polarization state and the attendant expansion of the viewing cone. The intended purpose of the diagram is

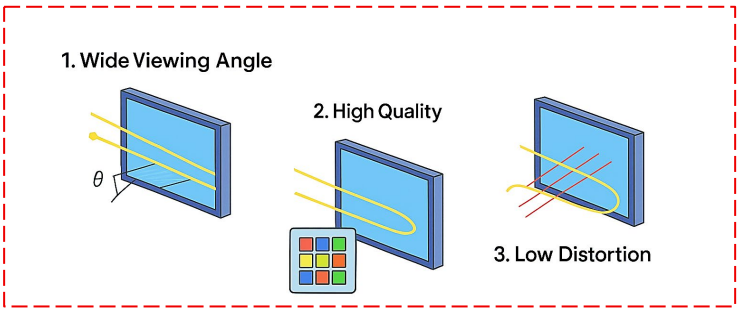

Fig. 10. Schematic representation of the role of birefringence in viewing angle compensation and image quality enhancement in polymeric displays.

to clarify the causal linkage between the supramolecular organization of the polymer films, the deliberate manipulation of birefringence, and the tangible improvements realized in state-of-the-art display performance. Such conceptual frameworks are instrumental in guiding the rational design of film compositions and processing protocols to forestall unwanted optical effects, be they angularly dependent chromaticity shifts or luminance roll-off [91].

8. Conclusions and future perspectives

Birefringence in polymers and polymeric nanocomposites constitutes a direct manifestation of structural anisotropy operative at both the molecular and mesoscopic scales, representing one of the most fundamental and technologically significant optical characteristics of these materials. This review has demonstrated that the origin of this behavior is rooted in three principal factors: (1) the preferential orientation of polymer chains induced by mechanical processes such as uniaxial drawing, injection molding, or extrusion, which is quantitatively described through the stress-optical coefficients (C_r and C) and the Hermans orientation parameter (f); (2) the application of external electric (Pockels effect) and magnetic fields, which, via the mechanism of induced polarization, engender transient or permanent optical anisotropy; and (3) the deliberate incorporation of shape-anisotropic nanofillers (e.g., nanotubes and nanoplatelets), whose spatial organization imposes form birefringence upon the composite architecture. This inherent tunability enables the precise control and engineering of light propagation within the material, thereby positioning polymers as a compelling platform for the design of lightweight, flexible, and cost-effective photonic materials.

The Lorentz–Lorenz equation, which serves as a critical bridge between molecular-scale polarizability and the macroscopic refractive index, together with the Abbe number as a metric of chromatic dispersion, constitute two indispensable parameters in the rational engineering of polymeric optical media. While a traditional inverse correlation has historically constrained the simultaneous achievement of high refractive index and high Abbe number, astute molecular design exemplified by the strategic introduction of tailored aromatic moieties or heavy atoms affords a viable pathway to transcend this empirical limitation.

Advanced characterization methodologies have proven essential for the precise quantification and spatial mapping of birefringence in complex polymeric systems. Techniques such as spectroscopic ellipsometry and Mueller-matrix ellipsometry enable the decoupling of the ordinary and extraordinary refractive indices (n_o and n_e) with exceptional accuracy, even in multilayer thin-film architectures. Complementarily, polarized optical microscopy (POM) and birefringence imaging provide spatially resolved maps of optical retardation and fast-axis orientation, facilitating the direct visualization of stress-induced anisotropy, molecular alignment, and morphological textures. For dynamic and in situ investigations, rheo-optical instrumentation and photoelastic modulation allow the real-time monitoring of birefringence evolution under mechanical load, thermal cycling, or electromagnetic stimuli. The integration of these metrological tools with robust optical modeling frameworks such as the Maxwell–Garnett effective medium theory for nanocomposites has significantly advanced our ability to correlate macroscopic optical signatures with underlying microstructural features, thereby informing the iterative design and optimization of high-performance photonic materials.

The interplay between the polymer matrix and dispersed nanoparticulate inclusions introduces additional degrees of complexity and opportunity in the engineering of birefringent response. The state of nanoparticle dispersion, the nature of the interfacial region, and the presence of surface functionalization profoundly influence the local chain conformation and the resultant optical anisotropy. For instance, well-dispersed, surface-passivated nanofillers can augment the free volume of the matrix, thereby accelerating the photoisomerization kinetics of azobenzene-containing polymers and enhancing the magnitude of photoinduced birefringence. Conversely, nanoparticle agglomeration or the formation of percolated networks can lead to undesirable light scattering, depolarization, and the introduction of spurious birefringent artifacts. In systems where magnetic nanoparticles are aligned under an external field and subsequently locked into a cured matrix, the resulting chain-like assemblies give rise to pronounced Cotton–Mouton birefringence, enabling the fabrication of solid-state quarter-wave retarders that operate without the need for a biasing field. A comprehensive understanding of these particle–matrix interactions is therefore paramount for harnessing the full potential of nanohybrid materials in adaptive optics and sensing applications.

The long-term stability and environmental resilience of birefringent polymeric materials represent critical considerations for their successful deployment in practical devices. Process-induced molecular orientation, while often desirable for achieving a specific Δn, can be susceptible to thermal relaxation, particularly when the material is operated near or above its glass transition temperature (T_g). The gradual loss of orientational order through segmental motion leads to a concomitant decay in birefringence, a phenomenon that can compromise the performance and service lifetime of optical components such as retardation films and waveguide claddings.

Strategies to mitigate this thermal instability include the incorporation of physical or chemical cross-links to restrict chain mobility, the utilization of high T_g polymer backbones with intrinsically rigid architectures, and the stabilization of oriented domains through strain-induced crystallization or the formation of interpenetrating networks. Furthermore, in photoresponsive systems based on azobenzene chromophores, the long-term photostability and resistance to photobleaching of the active moiety are essential for maintaining consistent cyclic performance in optical switching and data storage applications. Addressing these degradation pathways through informed materials chemistry and robust device packaging is essential for translating laboratory demonstrations into commercially viable and durable photonic technologies.

In the display and optoelectronics industry, the precise manipulation of birefringence in polymeric films has been instrumental in the development of retardation films and compensation layers essential to contemporary LCD and OLED architectures. The wavelength- and angle-resolved calibration of the refractive index differential (Δn) directly enhances image fidelity, suppresses parasitic light leakage, and broadens the angular viewing envelope of modern displays. Moreover, the integration of nanohybrid constructs and photoresponsive polymers has enabled the emergence of intelligent display elements capable of dynamically modulating their color or polarization state in direct response to external environmental stimuli.

Looking ahead, the trajectory of research in this domain is increasingly oriented toward the realization of smart materials with multi-field tunable birefringence systems engineered to exhibit a coordinated and reversible optical response to a confluence of triggers, including light, heat, and electric or magnetic fields. The synergistic convergence of nanophotonics, electroactive polymer science, and first-principles quantum mechanical modeling of the dielectric response is poised to catalyze the development of a new generation of optical materials and devices. The anticipated impact of these innovations is expected to extend well beyond the traditional confines of optical telecommunications, with transformative potential envisioned for applications in biosensing, next-generation renewable energy technologies, and the nascent architectures of future optical computing.

CRediT authorship contribution statement

Ali Borchloo: Conceptualization, Methodology, Investigation, Writing original draft, Writing review & editing, Visualization, Data curation, Resources, Project administration.

Data availability

No new data were created or analyzed in this study. Data sharing does not apply to this article.

Declaration of competing interest

The authors declare no competing interests.

Funding and acknowledgment

This research did not receive any specific grant from funding agencies in the public, commercial, or not-for-profit sectors.

References

[1] J.J. Zhao, Q. Zhang, S.F. Li, H. Gu, S. Liu, et al., Record-High Birefringence with Ultralow Dichroic Loss Realized by Cation-Templated Engineering Ordered Assembly of Linear Birefringent-Active Unit, Adv. Funct. Mater. 36 (2026) e76025. https://doi.org/10.1002/adfm.76025.

[2] K.K. Ahmed, D.Q. Muheddin, P.A. Mohammed, G.S. Ezat, A.R. Murad, et al., A brief review on optical properties of polymer Composites: Insights into Light-Matter interaction from classical to quantum transport point of view, Results Phys. 56 (2024) 107239. https://doi.org/10.1016/j.rinp.2023.107239.

[3] J.J. Zhao, S.F. Li, J. Chen, H. Huang, B. Zhang, D. Yan, Cationic-Dual-Modulated Linear and V-Shaped Birefringent-Active Unit Generates Remarkable Birefringence, Adv. Opt. Mater. 14 (2025) e03184. https://doi.org/10.1002/adom.202503184.

[4] A. Kausar, I. Ahmad, T. Zhao, O. Aldaghri, K.H. Ibnaouf, M.H. Eisa, Multifunctional Polymeric Nanocomposites for Sensing Applications—Design, Features, and Technical Advancements, Crystals. 13 (2023) 1144. https://doi.org/10.3390/cryst13071144.

[5] Y. Zhang, Y. Cai, Y. Zhou, Y. Liu, H. Hu, T. Lin, Effects of Epoxy Molecular Structure on Photoelastic Properties for Micro-Stress Optical Measurement, J. Appl. Polym. Sci. 143 (2025) e70062. https://doi.org/10.1002/app.70062.

[6] P. Melnikov, A. Bobrov, Y. Marfin, On the Use of Polymer-Based Composites for the Creation of Optical Sensors: A Review, Polymers (Basel). 14 (2022) 4448. https://doi.org/10.3390/polym14204448.

[7] M.Z. Zhang, C.L. Hu, Y.W. Shan, J.G. Mao, Achieving High-Birefringence Thiophosphates From Low Polarizability Anisotropy Units by an Axial Linear Matching Strategy, Adv. Opt. Mater. 14 (2026) e71305. https://doi.org/10.1002/adom.71305.

[8] D. Zhang, D. Lyu, S. Pathania, J. Luo, Modular Synthesis and Interface Engineering of Guest–Host Polymers Containing Highly Asymmetrical Push–Pull Heptamethines for Electro-Optics, ACS Appl. Opt. Mater. 4 (2026) 877–888. https://doi.org/10.1021/acsaom.5c00664.

[9] J. Mazuryk, P. Paszke, D.A. Pawlak, W. Kutner, P.S. Sharma, Fabrication, Characterization, and Sensor Applications of Polymer-Based Whispering Gallery Mode Microresonators, ACS Sens. 10 (2025) 5314–5338. https://doi.org/10.1021/acssensors.5c00057.

[10] D. Zang, W. Liu, Y. Li, Y. Yang, Cholesteric Liquid Crystal Polymer Network/Patterned Quarter-Waveplate Composite Film for Anti-Counterfeiting, J. Polym. Sci. 64 (2026) 3125–3133. https://doi.org/10.1002/pola.70211.

[11] S. Yoo, S. Park, Y. Jeon, S. Song, J. Lim, Modular 9,9-Substituted Fluorene Cardo Design for Thermoplastic High-Refractive-Index Polymers with Low Birefringence, Macromolecules. 59 (2026) 4188–4197. https://doi.org/10.1021/acs.macromol.5c03159.

[12] D. Yan, Z. Wang, X. Li, L. Zhang, J. Li, 3D-Printed Linear-Polarization Multiplexed Metasurface for Independent Terahertz Focusing and Orbital Angular Momentum Beam Generation, IEEE J. Sel. Top. Quantum Electron. 32 (2026) 1–11. https://doi.org/10.1109/jstqe.2026.3676207.

[13] H. Jamil, M. Faizan, M. Adeel, T. Jesionowski, G. Boczkaj, A. Balciunaite, Recent Advances in Polymer Nanocomposites: Unveiling the Frontier of Shape Memory and Self-Healing Properties-A Comprehensive Review, Molecules. 29 (2024) 1267. https://doi.org/10.3390/molecules29061267.

[14] K. Xie, Z. Bai, W. Huang, J. Qi, T. Lin, et al., Unveiling the Superior Birefringence Property of a Record-Birefringent Crystal with Unique Building Block, Angew. Chem. Int. Ed. Engl. 65 (2026) e24729. https://doi.org/10.1002/anie.202524729.

[15] C.-H. Xie, L. Liu, X.-M. Jiang, B.-W. Liu, G.-C. Guo, Anion-Centered Engineering for Simultaneously Enhancing Birefringence and Band Gap in Chalcogenides, Chem. Mater. 38 (2026) 1478–1485. https://doi.org/10.1021/acs.chemmater.5c03056.

[16] X. Wang, H. Sha, Z. Wang, F. Wang, S. Li, J. Zhang, Coordination-Induced Amplification of Birefringence and Nonlinear Optical Response in a Chiral Metal-Organic Framework, Angew. Chem. Int. Ed. Engl. 65 (2026) e16178. https://doi.org/10.1002/anie.202516178.
[17] A. Tagaya, Birefringence of Polymer, in: Encyclopedia of Polymeric Nanomaterials, Springer, Berlin, Heidelberg. (2013) 1–6. https://doi.org/10.1007/978-3-642-36199-9_116-1.
[18] D.O. Dorohoi, M. Postolache, C.D. Nechifor, D.G. Dimitriu, Review on Optical Methods Used to Characterize the Linear Birefringence of Polymer Materials for Various Applications, Molecules. 28 (2023) 2955. https://doi.org/10.3390/molecules28072955.
[19] J.A. van den Born, R. Landman, D.S. Doelman, F. Snik, Y. Nishie, et al., Vector Apodizing Phase Plates for the ELT: From prototype to final optics for METIS and MICADO, arXiv preprint arXiv:2607.03119 (2026). https://doi.org/10.48550/arXiv.2607.03119.
[20] A. Tiwari, A. Zhang, S. Sburlati, J. Freudenthal, O. Arteaga, et al., Anomalous Circular Birefringence in Isomorphous Mixed Crystals, Adv. Funct. Mater. 36 (2026) e74854. https://doi.org/10.1002/adfm.74854.
[21] H. Tao, Controlling self-assembly of cellulose nanocrystals for multiphase colloids and chiral photonics, Doctoral Thesis, Aalto University. (2026).
[22] S. Ando, Polymers for Optical Communications, in: M.K. Mishra, I. Tomita, K. Takagi (Eds.), Polymers for Optical Communications, CRC Press. (2025). https://doi.org/10.1201/9780367694265-EPPMPT75-1.
[23] R. Takahashi, K. Kojima, M. Yamaguchi, Y. Okumura, H. Matsukizono, H. Kikuchi, Ultrafast Electro-Optical Response of Polymer-Dispersed Liquid Crystals with Ferroelectric Nematic Liquid Crystal in Light Transmission to Light Scattering Switching, Macromol. Mater. Eng. 311 (2025) e00369. https://doi.org/10.1002/mame.202500369.
[24] H. Sun, Y.W. Yang, Y.K. Li, Z.N. Zhou, R. Tsunashima, et al., Supramolecular Rotor Assemblies Exhibiting Thermally Driven Shear-Dominated Transformation and Birefringence Switching, Adv. Funct. Mater. 36 (2025) e26703. https://doi.org/10.1002/adfm.202526703.
[25] N. Sashi, E. Yoshida, H. Maeda, R. Takahashi, K. Hatakeyama-Sato, et al., Humidity-robust semi-aromatic polyimides with cyclohexyl-substituted double-decker-shaped silsesquioxane exhibiting low dielectric losses at 10-20 GHz, Commun. Mater. 7 (2026) 163. https://doi.org/10.1038/s43246-026-01217-7.
[26] N. Rahayu, F.N. Ramadhani, Performance of optical fibers birefringence and its effect on wavelength, Sci. Technol. Commun. J. 6 (2026) 135–140. https://doi.org/10.59190/stc.v6i2.321.
[27] A. Puro, Birefringence in inhomogeneous dichroic materials, Recent Advances in Experimental Mechanics, CRC Press. 1 (1994).
[28] A. Pradeep, Y. Montelongo, J.S. Ma, Z. Xu, T. Wang, et al., From Millimeters to Microns: A Hybrid Strategy for Reconfigurable Liquid-Crystal Patterning, Small Methods. 10 (2026) e01892. https://doi.org/10.1002/smtd.202501892.
[29] S. Pagidi, R. Manda, V.N. Rao, Q. Chen, F. Wang, et al., Enhanced Electro-Optic Switching in High-Dielectric TiO2-Doped Nanoscale Liquid Crystal Droplets, Adv. Mater. Technol. 11 (2025) e01555. https://doi.org/10.1002/admt.202501555.
[30] K. Nakano, A. Shishido, S. Kubo, I. Tomita, K. Takagi, Liquid-Crystalline Polymers, CRC Press. (2026). https://doi.org/10.1201/9780367694265-EPPMPT188-1.
[31] K. Nakano, M. Aizawa, K. Hisano, Y. Naka, T. Fukushima, et al., Recyclable Cross-Linking of Liquid-Crystalline Polymers Grafted from Nanorod Surfaces by Atom Transfer Radical Polymerization, ACS Appl. Polym. Mater. 8 (2026) 4705–4712. https://doi.org/10.1021/acsapm.5c04522.
[32] A. Maulik, R. De, J. Ralhan, V.C. Chandran, S. Deshmukh, et al., Azobenzene Photoswitch in Asymmetric Polydiacetylenes Dictates Molecular Ordering and Soft-Crystalline Transitions, Chem. Asian J. 21 (2026) e00926. https://doi.org/10.1002/asia.202500926.
[33] J. Mao, J. Myers, M. Cakmak, Hydrogen-Bond Mediated Structural Evolution and Mechano-Optical Anisotropy During Drying and Uniaxial Stretching of Poly(Vinyl Alcohol) Films: Effect of Molecular Weight, Polym. Eng. Sci. 66 (2025) 172–189. https://doi.org/10.1002/pen.70199.
[34] M.J. Lopera, Y. Nie, C. Trujillo, H. Ottevaere, Classification of microplastics in field-collected stream water using a submersible single-shot lensless polarimetric holographic system, Opt. Express. 34 (2026) 19094–19108. https://doi.org/10.1364/OE.597670.
[35] J.E. Mark, Physical Properties of Polymers Handbook, 2nd ed., Springer, New York. (2007). https://doi.org/10.1007/978-0-387-69002-5.
[36] Y. Long, X. Dong, L. Qi, L. Luan, Z. Ren, et al., Halogen-Substitution-Modulated Lone-Pair Orientation in Sb(H2PO2)2X (X = Cl, F) for Enhanced UV Birefringence, Crys. Growth Des. 26 (2026) 5586–5593. https://doi.org/10.1021/acs.cgd.6c00518.
[37] X. Liang, H. Xia, W. Peng, X. Zhang, Y. Ma, et al., Kaleidoscopic stress-colored birefringent metamaterial for digital multiplexed encryption, Matter. 9 (2026) 102435. https://doi.org/10.1016/j.matt.2025.102435.
[38] J. Lee, Y.W. Kim, H. Chang, H. Hugonnet, C. Oh, et al., Incoherent dielectric tensor tomography for quantitative three-dimensional measurement of biaxial anisotropy, Nat. Photon. 20 (2026) 773–782. https://doi.org/10.1038/s41566-026-01897-0.
[39] Q. Li, R. Zhu, K. Liu, J. Jiang, T. Liu, Z. Ding, Local Birefringence Imaging by Similar Mueller Matrix Averaging Method in Catheter-Based Polarization-Sensitive Optical Coherence Tomography, Chem. Biomed. Imaging. 4 (2026) 1163–1172. https://doi.org/10.1021/cbmi.5c00203.
[40] B. Li, Z. Zhang, J. Fan, Y. Hao, K. Chen, X. Zhang, Fatigue Behavior and Multiscale Structural Evolution of Polyamide 66 Industrial Fiber Under Cyclic Loading, Polym. Eng. Sci. 66 (2025) 2232–2243. https://doi.org/10.1002/pen.70348.
[41] Z. Lei, W. Guo, X. Fang, Z. Tan, H. Xue, et al., Uniaxial tensile strain-insensitive and zero-birefringence cellulose acetate films via atom-economic isocyanate modification, Carbohydr. Polym. 382 (2026) 125232. https://doi.org/10.1016/j.carbpol.2026.125232.
[42] Y. Kuga, Y. Ino, K. Yamauchi, S. Sode, O.C. Namli, R. Furukawa, Polymer optical fiber using zero–zero birefringence core, Jpn. J. Appl. Phys. 65 (2026) 017002. https://doi.org/10.35848/1347-4065/ae2c2b.
[43] K. Rusek, A.M. El-Naggar, A. Albassam, G. Lakshminarayana, M. Kolcun, et al., Laser-induced birefringence in La–Ga–S–O–Gd glass polymer nanocomposites, J. Mater. Sci.: Mater. Electron. 27 (2016) 6745–6749. https://doi.org/10.1007/s10854-016-4623-1.
[44] M. Kobayashi, W.K.A. Worby, M. Kawaguchi, Y. Yokoyama, S. Ichihara, Y. Tagawa, Extending flow birefringence analysis to combined extensional–shear flows via Jeffery–Hamel flow measurements, Exp. Therm. Fluid Sci. 174 (2026) 111708. https://doi.org/10.1016/j.expthermflusci.2026.111708.
[45] M. Postolache, D.G. Dimitriu, C.D. Nechifor, S. Condurache Bota, V. Closca, D.O. Dorohoi, Birefringence of Thin Uniaxial Polymer Films Estimated Using the Light Polarization Ellipse, Polymers (Basel). 14 (2022) 1063. https://doi.org/10.3390/polym14051063.
[46] M.M. Khashoqji, T.S. Alraddadi, A.M. Munshi, M.D. Sharahili, H.A. Alghasham, et al., Opto-Mechanical Characterization and Antimicrobial Performance of iPP/TiO(2) and iPP/Ag Nanocomposite Fibers: A Combined Stokes Polarimetry and Birefringence Analysis, Luminescence. 41 (2026) e70464. https://doi.org/10.1002/bio.70464.
[47] T. Kawano, K. Inoue, M. Shiratake, N. Kato, High-refractive-index, low-birefringence polymers with wavelength selectivity for AR/VR devices, Proceedings. 13821 (2026) 197–200. https://doi.org/10.1117/12.3089628.

[48] A. Hashim, Q. Hadi, Structural, electrical and optical properties of (biopolymer blend/titanium carbide) nanocomposites for low cost humidity sensors, J. Mater. Sci.: Mater. Electron. 29 (2018) 11598–11604. https://doi.org/10.1007/s10854-018-9257-z.
[49] M. Jo, Y.C. Shi, In vitro mammalian intestine mucosal enzymatic digestion of starch spherulites formed from debranched waxy maize and high-amylose maize starches, Carbohydr. Polym. 381 (2026) 125151. https://doi.org/10.1016/j.carbpol.2026.125151.
[50] L. Jin, W. Mo, Z. Wang, W. Hong, Vortex-Enabled Nonreciprocal Circularly Polarized Luminescence in Achiral Polymer Systems, Adv. Funct. Mater. 36 (2025) e21524. https://doi.org/10.1002/adfm.202521524.
[51] T. Inaoka, T. Hattori, M. Yamaguchi, Effect of Long-Chain Branched High-Density Polyethylene on Shear-Induced Crystallization of Polypropylene, Polym. Eng. Sci. 66 (2026) 5701–5712. https://doi.org/10.1002/pen.70600.
[52] H.R.S. Mahdavi, E. Mohajerani, M. Mohseni, Y. Aghili, A novel approach to analyze photoinduced effects in a DR1 dye-doped hybrid nanocomposite film, J. Sol-Gel Sci. Technol. 52 (2009) 82–87. https://doi.org/10.1007/s10971-009-2000-8.
[53] R.S. Herrera Restrepo, I.H. Tejedor Garcia, M.G. Scarfo, N. Bouzari, N. Rajabi, et al., Porous Hybrid Soft Actuators From Liquid Crystal Networks and Lyotropic Chromonic Liquid Crystal Templated Hydrogels, Adv. Mater. 38 (2026) e16677. https://doi.org/10.1002/adma.202516677.
[54] P.H. Guo, X. Zhang, M. Mutailipu, S. Zhao, N. Zhang, et al., Ultrawide Bandgap and Record-High Birefringence in a Covalent Beryllium-Organic Framework, J. Am. Chem. Soc. 148 (2026) 18066–18073. https://doi.org/10.1021/jacs.6c01919.
[55] F. Guo, L. Chen, J. Yu, Y. Li, Y. Sun, Z. Gao, Ultra-Small Birefringence Continuous-Tuning and Full-Band Zero-Order Waveplate Devices, Adv. Opt. Mater. 14 (2025) e02910. https://doi.org/10.1002/adom.202502910.
[56] S.B. Aziz, M.A. Brza, M.M. Nofal, R.T. Abdulwahid, S.A. Hussen, et al., A Comprehensive Review on Optical Properties of Polymer Electrolytes and Composites, Materials (Basel). 13 (2020) 3675. https://doi.org/10.3390/ma13173675.
[57] S.K. Yesodha, C.K. Sadashiva Pillai, N. Tsutsumi, Stable polymeric materials for nonlinear optics: a review based on azobenzene systems, Prog. Polym. Sci. 29 (2004) 45–74. https://doi.org/10.1016/j.progpolymsci.2003.07.002.
[58] M. Ghandoura, C. Sudjaa, A. Sureshkumara, S. Pernona, N. Coulona, et al., 3D printing of micron-scale tapered optical fibers made from bio-based organic materials: multiple physical and optical characterizations, towards a new form of integrated photonic, Proceedings. 14082 (2026) 140820K–140821. https://doi.org/10.1117/12.3092699.
[59] M. Cheng, W. Zhang, W. Jin, A.R. Oganov, Z. Yang, S. Pan, Hydroxyl-induced structural reconstruction: two new potassium hepta-borates with deep-UV transparency and enhanced birefringence, Inorg. Chem. Front. 13 (2026) 1006–1012. https://doi.org/10.1039/d5qi02044a.
[60] D. Anestopoulos, G. Tsigaridas, P. Persephonis, V. Giannetas, I. Spiliopoulos, et al., Electro-optic characterization of two novel organic materials in thin polymeric films, Chem. Phys. Lett. 390 (2004) 98–103. https://doi.org/10.1016/j.cplett.2004.03.130.
[61] N.G. Sultanova, S.N. Kasarova, I.D. Nikolov, Characterization of optical properties of optical polymers, Opt. Quantum Electron. 45 (2012) 221–232. https://doi.org/10.1007/s11082-012-9616-6.
[62] D. Chen, Z.S. Davidson, B.P. Radka, S. Elhadj, L.C. Chien, The Evolution of Laser-Induced Damage Patterns in Polymer Stabilized Liquid Crystals: Insights From Morphological Characterization and Thermo-Driven Simulations, Adv. Opt. Mater. 14 (2026) e03418. https://doi.org/10.1002/adom.202503418.
[63] C.A. Chen, Y. Li, C. Jin, S. Lee, Z. Yang, K.M. Ok, Density-Compensated Polarizability Anisotropy for Record Birefringence in Short-Wavelength Ultraviolet Inorganic Crystals, J. Am. Chem. Soc. 148 (2026) 11187–11195. https://doi.org/10.1021/jacs.5c23008.
[64] V. Calabrese, Emergent Interpolymer Interactions in Flowing Polymer Solutions, ACS Macro. Lett. 15 (2026) 368–379. https://doi.org/10.1021/acsmacrolett.6c00010.
[65] I.E.G. Balderas, A.P. Kondratov, V.Y. Vereshchagin, A.Y. Pogiba, Optical Properties of Colorless Polymer Coatings on the Mirrored Surface of Containers, Phys. Solid State. 68 (2026) 283–289. https://doi.org/10.1134/s1063783425603212.
[66] C. Inui, H. Kura, T. Sato, Y. Tsuge, S. Shiratori, et al., Preparation of nanocomposite for optical application using ZnTe nanoparticles and a zero-birefringence polymer, J. Mater. Sci. 42 (2007) 8144–8149. https://doi.org/10.1007/s10853-007-1712-9.
[67] J.-M. Baek, S.-G. Park, J.-S. Ma, S. Bae, S.-W. Oh, A numerical study on a voltage-tunable quasi-broadband depolarizer enabled by periodic protrusion-induced liquid crystal reorientation, Curr. Appl. Phys. 90 (2026) 8–12. https://doi.org/10.1016/j.cap.2026.06.012.
[68] F. Ahmad, R.M. Khan, M. Ali, M. Luqman, M. Jamil, Investigation of interfacial and morphological characterization of dye-doped polymer-dispersed liquid crystal thin films via Langmuir surface tension techniques, Opt. Mater. 178 (2026) 118201. https://doi.org/10.1016/j.optmat.2026.118201.
[69] H.M. Abumelha, A.M. Alsharari, K.M. Alkhamis, M. Alshareef, K.A. Osra, et al., In-situ birefringence mapping of PET/TiO_2 nanocomposite fibers by dual-channel Fourier-transform polarizing interferometry: Drawing evolution and multi-factor environmental degradation, Optik. 352 (2026) 172810. https://doi.org/10.1016/j.ijleo.2026.172810.
[70] H.A. Hegazy, B.Y. Kim, I.G. Cho, J.-Y. Choi, G. Kim, et al., Fluorene-Derived High-Refractive-Index Polymers with Superior Optical and Thermal Properties for Advanced Optical Components, ACS Appl. Polym. Mater. 8 (2026) 1117–1131. https://doi.org/10.1021/acsapm.5c03904.
[71] J.-B. Tang, J.-Y. Wu, Z.-K. Ni, C. Tang, J. Lei, et al., Synergistic Flow-Stretch Coupling Enables an Oriented Network for High-Performance Polycarbonate with Superior High-Speed Deformation Resistance, Polymer. 363 (2026) 130565. https://doi.org/10.1016/j.polymer.2026.130565.
[72] A. Tagaya, Y. Koike, Compensation and control of the birefringence of polymers for photonics, Polym. J. 44 (2012) 306–314. https://doi.org/10.1038/pj.2011.141.
[73] S. Modiri, M. Mohseni, E. Mohajerani, I.A. Alidokht, Laser-induced birefringence of methyl red in a polymeric nanocomposite prepared by sol–gel method, Iran Polym. J. 21 (2012) 547–556. https://doi.org/10.1007/s13726-012-0060-z.
[74] J.M. Soulages, Flow birefringence and velocity measurements for polymer melts in a cross-slot flow channel, ETH-Diss. 17180, ETH Zurich. (2007). https://doi.org/10.3929/ethz-a-005397356.
[75] K. Lazarova, D. Christova, R. Georgiev, B. Georgieva, T. Babeva, Optical Sensing of Humidity Using Polymer Top-Covered Bragg Stacks and Polymer/Metal Thin Film Structures, Nanomaterials (Basel). 9 (2019) 875. https://doi.org/10.3390/nano9060875.
[76] J. Patrakka, V. Hynninen, P. Huttunen, Nonappa, Biopolymer Optical Fibers for High-Sensitivity Quantitative Humidity Monitoring, ACS Appl. Mater. Interfaces. 17 (2025) 49816–49828. https://doi.org/10.1021/acsami.5c10056.
[77] M.M. Mikhailov, V.A. Goronchko, S.A. Yuryev, A.N. Lapin, D.S. Fedosov, Optical properties of nanocomposites based on polypropylene modified by nanoparticles of oxide compounds, Results Opt. 16 (2024) 100696. https://doi.org/10.1016/j.rio.2024.100696.
[78] S. Hossain, Optical properties of polymers and their applications, M.S. Thesis, New Jersey Institute of Technology. (2019).
[79] S. Wu, J. Shen, J. Huang, Y. Wu, Z. Zhang, et al., Ag nanoparticle/azopolymer nanocomposites: In situ synthesis, microstructure, rewritable optically induced birefringence and

optical recording, Polymer. 51 (2010) 1395–1403. https://doi.org/10.1016/j.polymer.2010.01.062.
[80] K.K. Vardanyan, E.D. Palazzo, R.D. Walton, Nematic nanocomposites with enhanced optical birefringence, Liq. Cryst. 38 (2011) 709–715. https://doi.org/10.1080/02678292.2011.569760.
[81] R. Bouhfid, A.E.K. Qaiss, M. Jawaid (Eds.), Polymer Nanocomposite-Based Smart Materials: From Synthesis to Application, Woodhead Publishing. (2020). https://doi.org/10.1016/C2018-0-02562-1.
[82] M. Rubinstein, R.H. Colby, Polymer Physics, Oxford University Press, Oxford. (2003). https://doi.org/10.1093/oso/9780198520597.001.0001.
[83] J. Peretti, J. Biteau, J.-P. Boilot, F. Chaput, V.I. Safarov, et al., Remanent photoinduced birefringence in thin photochromic sol–gel films, Appl. Phys. Lett. 74 (1999) 1657–1659. https://doi.org/10.1063/1.123645.
[84] M. Wärnå, High refractive index monomers and polymers for optical applications, Aalto University. (2025).
[85] X. Rao, L. Zhao, L. Xu, Y. Wang, K. Liu, et al., Review of Optical Humidity Sensors, Sensors (Basel). 21 (2021) 8049. https://doi.org/10.3390/s21238049.
[86] R. Takahashi, Y. Ikura, D.R. King, T. Nonoyama, T. Nakajima, et al., Coupled instabilities of surface crease and bulk bending during fast free swelling of hydrogels, Soft Matter. 12 (2016) 5081–5088. https://doi.org/10.1039/c6sm00578k.
[87] S. Wang, X. Han, K. Li, Snapshot Multi-Wavelength Birefringence Imaging, Sensors (Basel). 24 (2024) 5174. https://doi.org/10.3390/s24165174.
[88] R. Honda, M. Ryu, J.L. Li, V. Mizeikis, S. Juodkazis, J. Morikawa, Simple multi-wavelength imaging of birefringence: case study of silk, Sci. Rep. 8 (2018) 17652. https://doi.org/10.1038/s41598-018-36114-8.
[89] G.G. Politano, C. Versace, Spectroscopic ellipsometry: advancements, applications and future prospects in optical characterization, Spectrosc. J. 1 (2023) 163–181. https://doi.org/10.3390/spectroscj1030014.
[90] G.E. Jellison, Jr., C.M. Rouleau, Determination of optical birefringence by using off-axis transmission ellipsometry, Appl. Opt. 44 (2005) 3153–3159. https://doi.org/10.1364/ao.44.003153.
[91] G.A. Lindsay, P.R. Ashley, M.C. Davis, A.J. Guenthner, M. Sanghadasa, M.E. Wright, New photonic and electronic polymers, Mater. Sci. Eng: B. 132 (2006) 8–11. https://doi.org/10.1016/j.mseb.2006.02.025.